Stem Cell Reports
Article

OPEN ACCESS

Stearoyl CoA Desaturase Is Essential for Regulation of Endoplasmic Reticulum Homeostasis and Tumor Growth in Glioblastoma Cancer Stem Cells

Kelsey Pinkham,[1,5] David Jaehyun Park,[1,2,5] Arsalan Hashemiaghdam,[1,2] Aleksandar B. Kirov,[1] Isam Adam,[1] Kamila Rosiak,[1] Cintia C. da Hora,[1,2] Jian Teng,[1,2] Pike See Cheah,[1,3] Litia Carvalho,[1,2] Gitali Ganguli-Indra,[4] Avalon Kelly,[4] Arup K. Indra,[4] and Christian E. Badr[1,2,*]

[1]Department of Neurology, Massachusetts General Hospital, Boston, MA 02129, USA
[2]Neuroscience Program, Harvard Medical School, Boston, MA 02129, USA
[3]Department of Human Anatomy, Faculty of Medicine and Health Sciences, Universiti Putra Malaysia, Seri Kembangan, Selangor 43400, Malaysia
[4]Department of Pharmaceutical Sciences, College of Pharmacy, Oregon State University, Corvallis, OR 97331, USA
[5]Co-first author
*Correspondence: badr.christian@mgh.harvard.edu
https://doi.org/10.1016/j.stemcr.2019.02.012

SUMMARY

Inherent plasticity and various survival cues allow glioblastoma stem-like cells (GSCs) to survive and proliferate under intrinsic and extrinsic stress conditions. Here, we report that GSCs depend on the adaptive activation of ER stress and subsequent activation of lipogenesis and particularly stearoyl CoA desaturase (*SCD1*), which promotes ER homeostasis, cytoprotection, and tumor initiation. Pharmacological targeting of SCD1 is particularly toxic due to the accumulation of saturated fatty acids, which exacerbates ER stress, triggers apoptosis, impairs RAD51-mediated DNA repair, and achieves a remarkable therapeutic outcome with 25%–100% cure rate in xenograft mouse models. Mechanistically, divergent cell fates under varying levels of ER stress are primarily controlled by the ER sensor IRE1, which either promotes *SCD1* transcriptional activation or converts to apoptotic signaling when SCD1 activity is impaired. Taken together, the dependence of GSCs on fatty acid desaturation presents an exploitable vulnerability to target glioblastoma.

INTRODUCTION

Nearly half of the patients diagnosed with glioblastoma (GBM), the most common malignant primary brain tumor, will die within a year (Ostrom et al., 2016), underlining the urgency for effective GBM therapies. Contributing to the genetic and phenotypic variability of GBM is a highly tumorigenic subpopulation of glioma stem-like cells (GSCs), which drives tumor initiation, growth, and recurrence (Lathia et al., 2015). Contingent on their inherent plasticity and survival cues that are not fully elucidated, these cells can survive and proliferate in a relatively hostile environment whereby hypoxia, acidic pH, and low nutrient levels prevail (Lathia et al., 2015). Such conditions induce cellular stress, in particular ER stress, which is known to promote pathogenesis in many diseases including cancer. ER stress, which is aberrantly high in tumors (Wang and Kaufman, 2014) and supports various hallmarks of cancer (Urra et al., 2016), is counteracted by the activation of the unfolded protein response (UPR), an adaptation signaling mechanism that enables tumor cells to survive under severe stress conditions (Urra et al., 2016). The UPR engages three signaling sensors, inositol-requiring enzyme 1 (*IRE1*), protein kinase RNA-like ER kinase (*PERK*), and activating transcription factor 6 (*ATF6*) (Ron and Walter, 2007), that act jointly to alleviate and resolve ER stress. UPR signaling also promotes tumor growth through various mechanisms, including the activation of lipid synthesis pathways (Cubillos-Ruiz et al., 2017). GBM presents an upregulated lipid metabolism characterized by increased activation of sterol regulatory element-binding protein 1 (SREBP1), a master transcriptional regulator of lipid synthesis (Guo et al., 2009), and an abundance of unsaturated fatty acids (UFAs) (Srivastava et al., 2010). One of the target genes regulated by SREBP1 is stearoyl coenzyme A (CoA) desaturase 1 (*SCD1*), a key enzyme responsible for the conversion of saturated fatty acids (SFAs) to UFAs, necessary for tumor proliferation in several malignancies (Igal, 2010), and the maintenance of lung and ovarian cancer stem cells (Li et al., 2017; Noto et al., 2013). A defining role of *SCD1* in GBM tumor initiation and growth, and the regulation mechanisms governing its activity, remain largely unexplored.

In this study, we demonstrate that persistent activation of ER stress promotes *SCD1* expression through the activation of IRE1 and SREBP1. We propose that, through its unique role of controlling intracellular levels of SFAs, SCD1 is an essential regulator of ER stress that confers a selective advantage and promotes survival of GSCs in their tumor microenvironment.

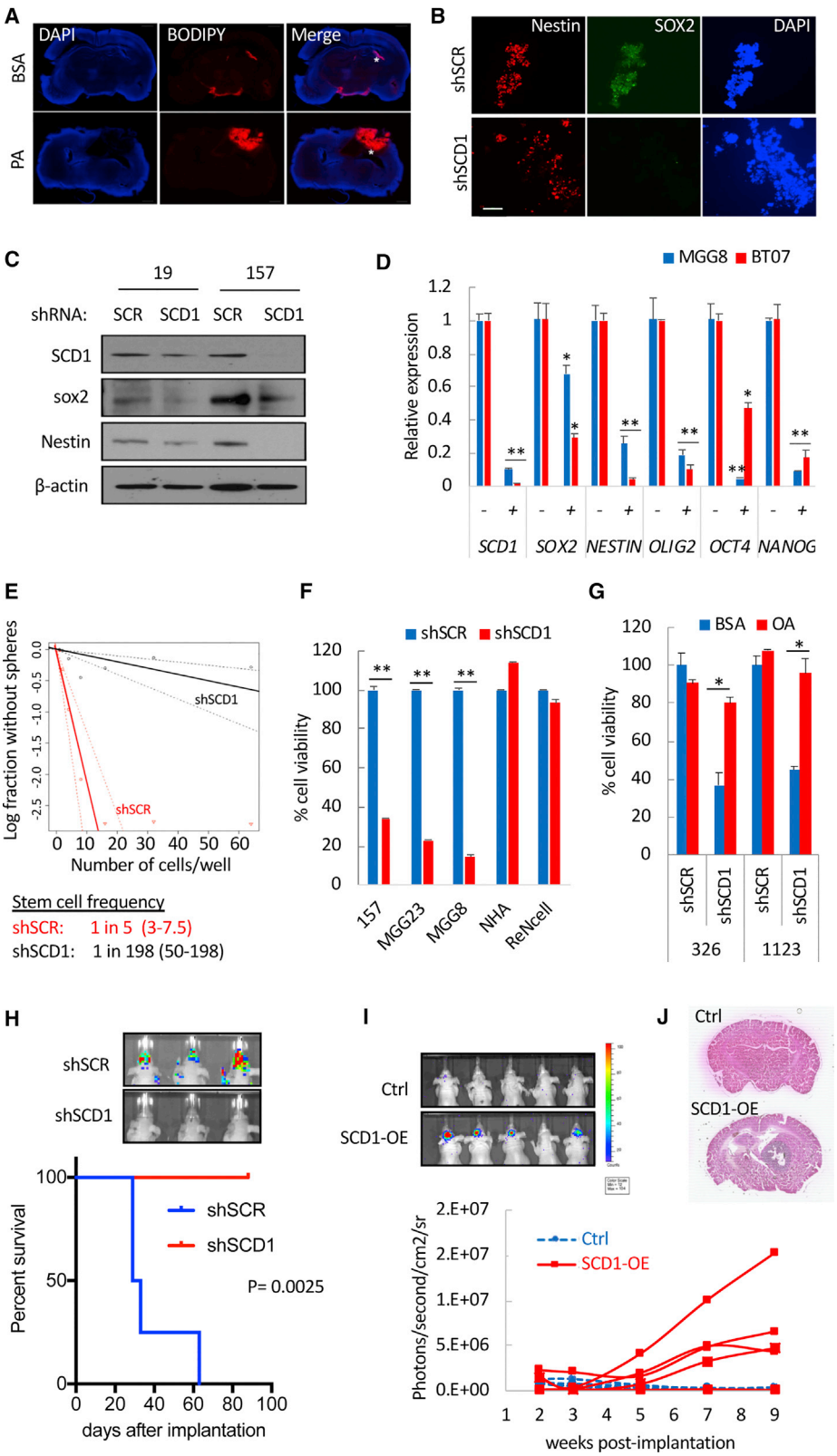

(legend on next page)

RESULTS

SCD1 Is a Therapeutic Target in Highly Proliferative GSC Populations

We have recently described a subpopulation of GSCs that escapes differentiation conditions and has enhanced stem cells properties, tumorigenic potential, and superior therapeutic resistance compared with the parental GSCs (Teng et al., 2017). To identify targeted inhibitors with increased toxicity toward this subpopulation that we termed floating cells (FCs), we have previously performed a small-scale inhibitors screen whereby GSCs and corresponding FCs were treated with target-selective inhibitors (Teng et al., 2017). Out of 141 compounds tested, only two inhibitors for *SCD1* and nicotinamide phosphoribosyltransferase (*NAMPT*), a recently identified therapeutic target for GBM (Tateishi et al., 2016), showed increased sensitivity to the FCs compared with the parental GSCs (Figure S1A). Intriguingly, while *SCD1* is a prominent target gene for SREBP1, *NAMPT* has also been reported to be positively regulated by this transcription factor (Rome et al., 2008). We primarily focused on *SCD1*, and first validated an increased sensitivity of FCs derived from two additional GSC lines to *SCD1* inhibitors (MK-8245 and CAY10566 [CAY]) compared with the parental GSCs (Figures S1B and S1C). Gene expression analysis showed increased expression of *SCD1* and other SREBP1 targets genes such as acyl-CoA synthetase short chain family member 2 (*ACSS2*), acetyl-CoA carboxylase α (*ACC1*), and fatty acid synthase (*FASN*) in the FC subpopulations (Figures S1D and S1E). An upregulated mRNA and protein expression of *SCD1* (Figures S1D and S1F), along with vulnerability to *SCD1* inhibitors, suggests an increased dependency of the FCs on *SCD1* activity. We have previously reported that FCs are characterized by aberrant activation of nuclear factor κB (NF-κB) and increased mesenchymal properties. Treatment of previously characterized proneural and mesenchymal GSCs (Mao et al., 2013) showed a clear sensitivity to the *SCD1* inhibitor in the latter subtype (Figure S1G). Overall, these findings suggest an increased expression and dependence on *SCD1* in highly tumorigenic GBM subpopulations.

SCD1 Is Essential for GSC Maintenance and *In Vivo* Tumor Initiation

Palmitic Acid (PA; C16:0) is the most abundant SFA in human serum and the direct substrate of *SCD1* (Carta et al., 2017). To functionally assess SCD1 activity *in vivo*, we tested whether PA supplementation could increase neutral lipid accumulation in GBM, detected using BODIPY, a fluorescent dye that stains neutral lipids. Indeed, tumor sections from mice receiving a daily dose of PA displayed a strong lipid staining (Figure 1A), suggesting that fractions of free PA are readily taken up by the tumor, desaturated by SCD1 before downstream processing into neutral lipids. Genetic silencing of *SCD1* with short hairpin RNA (shRNA) decreased the expression of the pluripotency markers *SOX2*, *NESTIN*, *OLIG2*, *OCT4*, and *NANOG* (Figures 1B–1D), as well as stem cell frequency (Figure 1E). Silencing of *SCD1* also decreased cell viability in five patient-derived GSCs (Figures 1F and 1G) but not in normal human astrocytes (NHAs) or immortalized neural stem cells (NSCs) maintained under serum-free conditions (Figure 1F). Supplying GSCs with oleic acid (OA; C18:1), the main product of SCD1, rescued from shSCD1-mediated cell death (Figure 1G). The role of SCD1 in tumor initiation was further evaluated by implanting GSCs expressing shSCR or shSCD1

Figure 1. SCD1 Is Essential for GSC Maintenance and Tumor Initiation

(A) Mice bearing 83-Fluc GSC tumors received daily injections over 7 days of BSA or PA (3 mg/kg of body weight). Representative brain sections were stained with BODIPY (red) and DAPI (blue). Asterisks depict the tumor injection site.

(B) Immunostaining for NESTIN, SOX2, and nuclei (DAPI) in 19-GSCs expressing shSCR or shSCD1 at day 7 after shRNA transduction. Scale bar, 100 μm.

(C) Immunoblot analysis of SCD1, SOX2, and NESTIN in GSCs expressing shSCR or shSCD1.

(D) Relative expression of stem cell markers determined by qPCR in GSCs transduced with shSCR or shSCD1 for 7 days.

(E) Stem cell frequency in 157 GSCs expressing shSCR or shSCD1 determined using the limited dilution analysis algorithm.

(F) Cell viability in three GSCs, NHA, and NSC expressing shSCR or shSCD1, at day 7 after transduction. Data is expressed as percentage of shSCR.

(G) GSCs (326 and 1123) expressing shSCR or shSCD1 were cultured in the presence of BSA or OA (50 μM). Cell viability was determined 7 days post transduction.

(H) 83-Fluc GSCs transduced with shCtrl or shSCD1 and intracranially implanted in mice (shCtrl, n = 4; sh*SCD1*, n = 6) after 24 h. Survival analysis is shown using Kaplan-Meier curves. p = 0.0025 (two-sided log-rank test). Representative Fluc imaging of brain tumors at day 10 post implantation is also shown.

(I) High-passage 157-Fluc GSCs (5×10^4) expressing control (Ctrl) or SCD1 (SCD1-OE) were implanted in the brain of nude mice (n = 5/group). Longitudinal Fluc imaging shown for individual mice in each group.

(J) H&E staining of brain sections of representative mice from both groups at day 135 post implantation.

*p < 0.05, **p < 0.001, Student's t test. See also Figure S2.

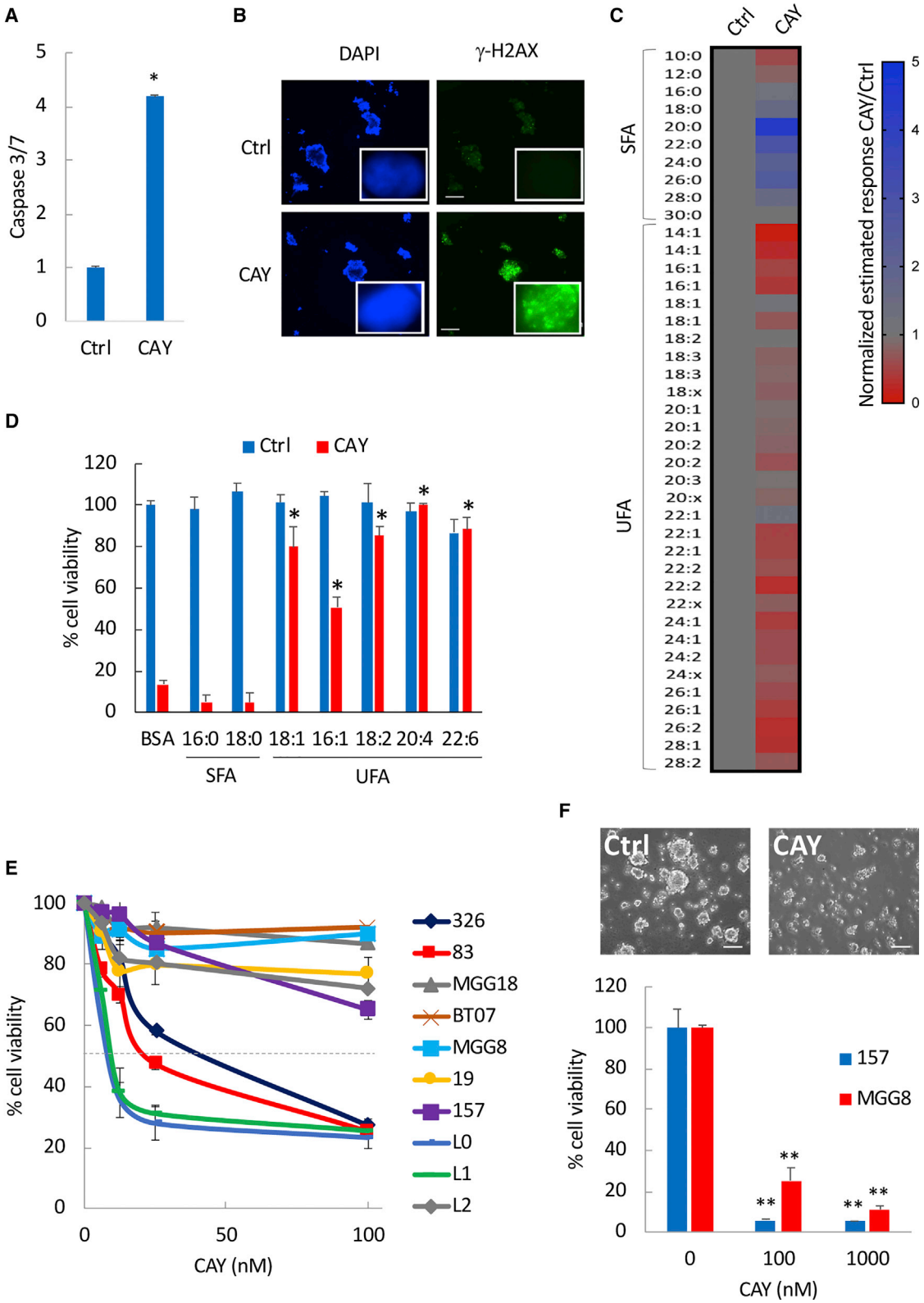

(legend on next page)

into the striatum of nude mice. Silencing of SCD1 completely prevented tumor growth as assessed by Firefly luciferase (Fluc) bioluminescence imaging as well as overall survival up to 150 days after implantation when the experiment was terminated (Figure 1H). Ectopic expression of SCD1 using a lentivirus system (SCD1-OE; Figure S2A) resulted in a greater than 5-fold increase in stem cell frequency in two GSCs (Figure S2B). We repeated these experiments in one GSC specimen that was propagated long-term as neurospheres (>50 passages) and presented a low stem cell frequency. Forced expression of SCD1 in these cells increased stem cell frequency (Figure S2C), cell proliferation (Figure S2D), and secondary neurosphere formation (Figure S2E). Following intracranial implantation of these high-passage GSCs in mice, four of five mice in the SCD1-OE group developed tumors that gradually grew over time (Figure 1I), and three of five succumbed to tumor burden by day 135 post implantation when this experiment was terminated (Figure S2F). None of the mice in the control arm developed any tumor detectable by Fluc imaging or H&E staining (Figures 1I, 1J, and S2F). In sum, SCD1 is essential for GSC maintenance and confers a tumor growth advantage *in vivo*.

Perturbation of SCD1 Activity Depletes GSCs Regardless of Their Genetic Background

We tested three pharmacological inhibitors of SCD1: PluriSIn, CAY, and the ACC1 inhibitor TOFA, which reportedly also inhibits SCD1 (Mason et al., 2012), and identified CAY as the most cytotoxic inhibitor with an average IC_{50} < 100 nM in different GSC specimens (Figure S3A and data not shown). GSCs treated with CAY showed increased caspase-3 and caspase-7 activities indicative of apoptotic cell death (Figure 2A), along with increased histone H2AX phosphorylation (γ-H2AX), a marker of DNA damage (Figure 2B). NHAs were indifferent to CAY treatment under serum-free conditions (Figure S3B). To confirm that CAY inhibits SCD1 activity, we analyzed fatty acid composition in GSCs treated with a control vehicle or CAY. We confirmed a decrease in UFAs (Figures 2C and S3C) and observed an overall increase of SFAs, which was more pronounced around C20:0–C26:0, thereby suggesting an accumulation of SFAs after CAY treatment (Figure 2C). Next, we performed rescue experiments after treatment with this inhibitor in the presence of SFAs (16:0; 18:0), monounsaturated FAs (18:1; 16:1; 18:2), and polyunsaturated FAs (20:4 n-6; 22:6 n-3). All of the UFAs tested almost completely protected against CAY-induced cell death (Figure 2D). We treated ten patient-derived GSCs with CAY and assessed short-term (4 days) and long-term (9 days) survival. We observed two different patterns of short-term response whereby four GSCs were highly sensitive to CAY-induced cell death with an IC_{50} < 60 nM, while six GSCs showed poor or no response (Figure 2E). However, long-term (9 days) treatment with CAY in this more resistant GSC subset (MGG8 and 157) resulted in >80% decrease in cell viability and neurosphere formation (Figure 2F). These results establish that inhibitors of SCD1 can effectively target patient-derived GBM cells in culture regardless of subtype.

Pharmacological Targeting of SCD1 Achieves a Strong Therapeutic Effect in GBM Mouse Models

To evaluate the therapeutic efficacy of SCD1 inhibition in GSCs xenograft mouse models, we elected to deliver CAY via the intranasal route, which allows bypassing of the blood-brain barrier (Chauhan and Chauhan, 2015). Mice were implanted with mesenchymal 83-Fluc GSCs and received a daily intranasal dose of 5 mg/kg of CAY (Figure 3A). Treatment with CAY did not cause any weight loss (Figure S3D) and resulted in an average decrease of 56% in Fluc signal at day 12 post-implantation (Figure 3B), along with decreased tumor proliferation assessed by Ki67 staining (Figure 3C). This translated into a significantly extended survival of 35 days in the treated group compared with 18 days for the control group (Figure 3D). Additionally, two of eight mice in the treated group were still alive at day 156 post implantation with no detectable tumors (Figure S3E). Under a similar experimental setup, mice receiving a lower dose of CAY (1.5 mg/kg) also showed a significantly extended survival of 22 days in the treated group compared with 16 days for the control group ($p = 0.0009$; Figure S3F). These experiments were repeated in mice bearing

Figure 2. Pharmacological Targeting of SCD1 Depletes GSCs

(A) Fold change in caspase-3/7 activation in 326 GSCs treated with CAY (200 nM).

(B) Immunostaining for γ-H2AX in CAY-treated GSCs. Scale bar, 200 μm. Representative images of single nuclei depicting γ-H2AX foci are also shown (inset).

(C) Heatmap representing the quantitative ratio of SFAs and UFAs in 83 CAY-treated GSCs relative to the untreated control. Values below or above 1 are indicative of decreased or increased fatty acids ratios, respectively.

(D) Cell viability in 83-GSCs treated with CAY (100 nM) in the presence of the indicated fatty acids.

(E) Cell viability at day 4 in ten GSC specimens treated with CAY at the indicated doses.

(F) Cell viability and representative bright-field micrographs of secondary spheres at day 9 in 157-GSCs treated with CAY (100 nM).

*$p < 0.05$, **$p < 0.001$, Student's t test. See also Figure S3.

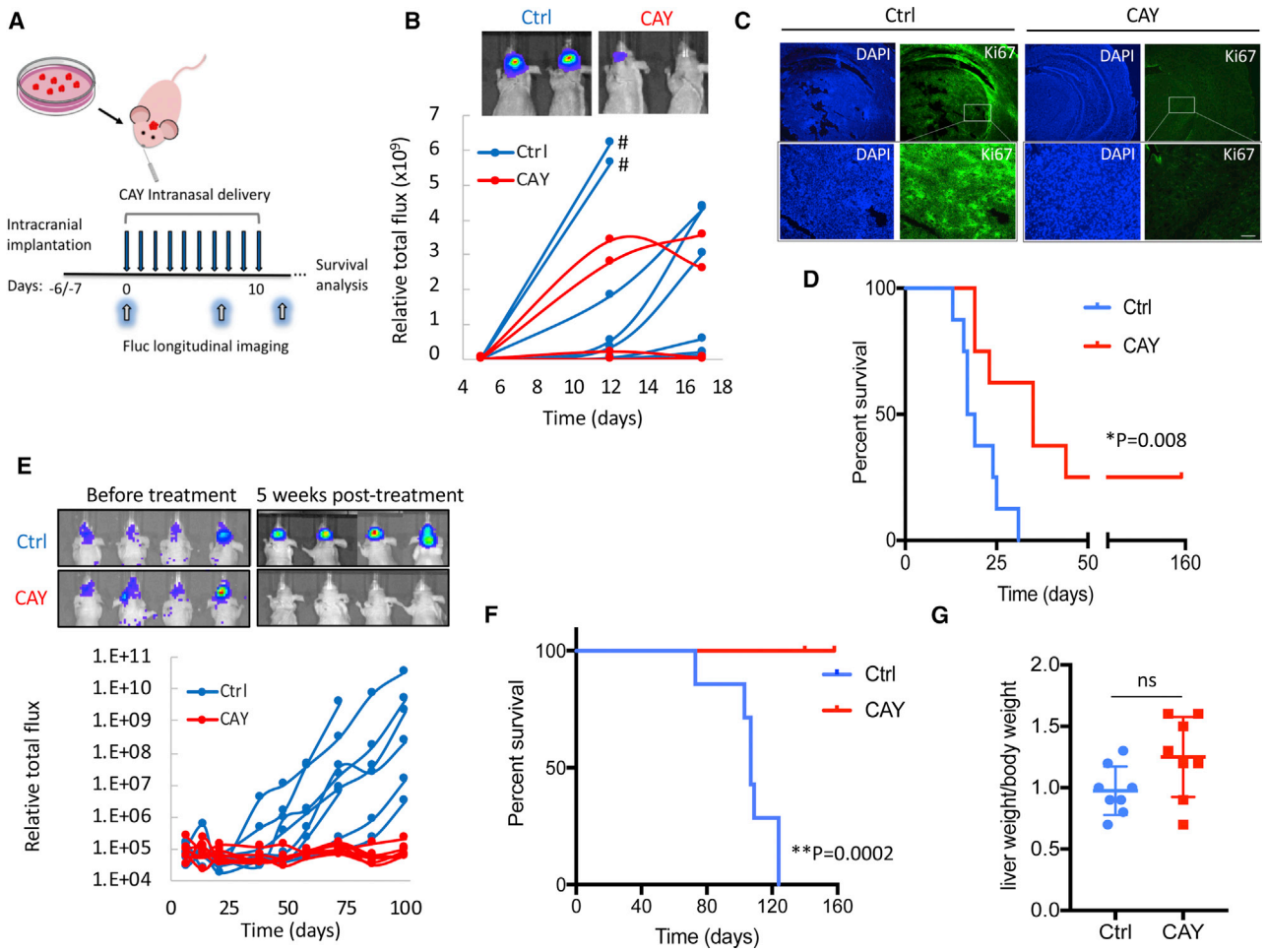

Figure 3. Therapeutic Targeting of SCD1 in Preclinical GBM Mouse Models

(A) Overview of experimental setup.

(B–D) Mice implanted with 83-Fluc GSCs (2×10^4; n = 8/group) received a daily intranasal dose of DMSO (Control) or CAY (5 mg/kg) for 10 days. (B) Overtime monitoring of tumor growth with Fluc imaging in individual mice from Ctrl and CAY-treated groups. Hash depicts the time of death due to tumor burden. (C) Ki67 immunostaining in one Ctrl and one CAY-treated mouse. Scale bar, 100 μm. (D) Kaplan-Meier curves showing median survival in both groups (*p = 0.008, two-sided log-rank test).

(E–G) Mice implanted with 157-Fluc GSCs (1×10^5; n = 8/group) were treated with vehicle or CAY (5 mg/kg). (E) Overtime Fluc imaging demonstrates the absence of tumor growth in all eight CAY-treated mice. (F) Survival curves in both groups (p = 0.0002; two-sided log-rank test). (G) The ratio of liver weight to the body weight in both experimental groups is shown. ns, non-significant by Student's t test.

See also Figure S3.

proneural 157-GSC brain tumors. All mice (8/8) in the control group showed growing tumors (Figure 3E) and eventually died from tumor burden (Figure 3F). Remarkably, none of the CAY-treated mice (0/8) had any detectable tumor and survived up to 158 days when the experiment was terminated (Figures 3E and 3F). We did not observe a significant change in liver weight following CAY treatment, suggesting an absence of hepatomegaly (Figure 3G). Therefore, intranasal delivery of CAY in patient-derived xenograft mouse models is a highly effective therapeutic strategy.

SCD1 Inhibition Exacerbates ER Stress through the Accumulation of SFAs

SFAs are known to induce ER stress (Volmer et al., 2013), hence the increased expression of the UPR transcripts *CHOP* and *sXBP1* in GSCs treated with PA (Figure S4A). Similarly, GSCs treated with CAY displayed a strong increase in the ER stress markers *BiP* (also known as *GRP78*), *CHOP*, *sXBP1*, and *GADD34* (Figure 4A), which was further accentuated over time (Figure 4A), in line with an increased accumulation of SFAs following SCD1 inhibition. Treatment with CAY also increased BiP (in two of the four GSCs tested)

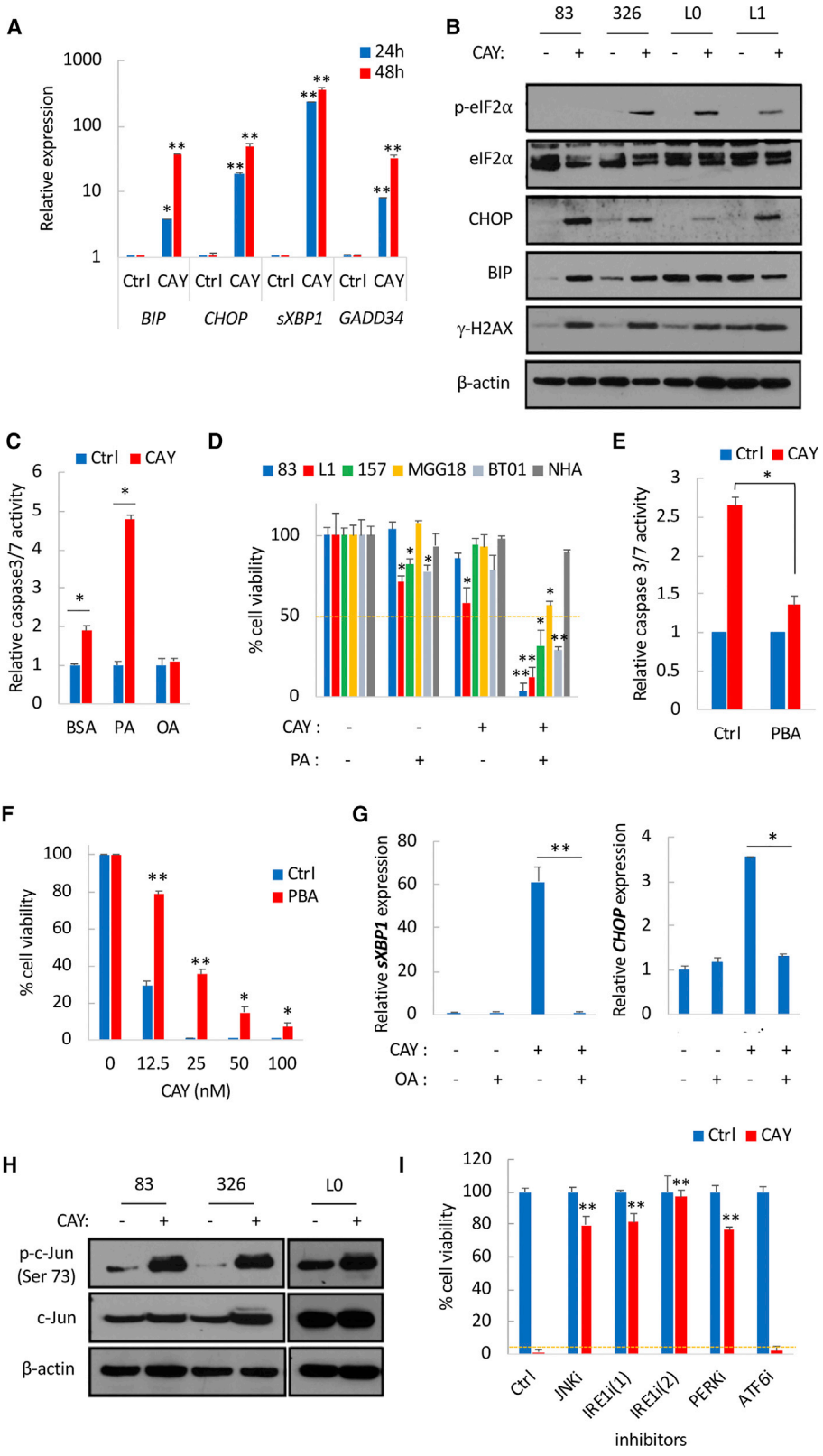

(legend on next page)

and CHOP proteins levels along with increased phosphorylation of eIF2α and γ-H2AX (Figure 4B). We hypothesized that SFA accumulation after CAY treatment primarily induces apoptotic cell death through an overwhelming ER stress response. The combination of CAY and a low dose of PA resulted in increased expression of *CHOP* and *sXBP1* transcripts (Figure S4B), as well as protein levels of BiP, CHOP, and γ-H2AX (Figure S4C). This combination also increased caspase-3/7 activities (Figure 4C) and cell death in GSCs but not in NHAs (Figure 4D). Similarly, silencing of SCD1 or treatment with a different SCD1 inhibitor increased PA-induced cytotoxicity (Figures S4D and S4E). The SFA stearic acid (SA; C18:0) also increased cell death when combined with CAY (Figure S4F). Alleviating ER stress with the chemical chaperone phenylbutyrate (PBA) significantly repressed caspase-3/7 activation (Figure 4E) and protected against SCD1 inhibition (Figure 4F). Further, azoramide, which protects against chemically induced ER stress (Fu et al., 2015), also significantly rescued mice from CAY-induced cytotoxicity (Figure S4G). Overall, these data demonstrate that targeting SCD1 results in chronic ER stress and renders GSCs susceptible to SFA-induced lipotoxicity.

SCD1-Mediated UFA Synthesis Mitigates ER Stress

We postulated that transcriptional activation of SCD1 and subsequent increase in UFAs mediates a cytoprotective function in GSCs. In line with the protective effect of OA following SCD1 targeting, treatment with OA reversed PA-induced cytotoxicity (Figure S5A) and prevented caspase-3/7 activation after treatment with CAY (Figure 4C). Importantly, OA suppressed *CHOP* and sXBP1 upregulation following CAY treatment (Figure 4G), thus suggesting that the protective role of UFAs such as OA after SCD1 inhibition is largely due to their potential role in alleviating ER stress. Ectopic expression of SCD1 reduced ER stress induced by PA or thapsigargin (Tg), as assessed by *BiP* and *sXBP1* mRNA expression (Figure S5B), and protected against PA-induced cytotoxicity (Figure S5C). Collectively, these results support that SCD1 acts as an essential regulator of ER stress to prevent prolonged UPR, thus favoring survival in GSCs.

Cell Death Caused by SCD1 Targeting Is Contingent on UPR Signaling

Persistent activation of UPR signals the inability of cells to adapt to ER stress, thus activating an apoptotic switch executed by CHOP or JNK (Szegezdi et al., 2006). Silencing of CHOP failed to protect against CAY-mediated cell death (Figures S5D and S5E). IRE1 kinase mediates proapoptotic signaling though the activation of JNK, which directly phosphorylates and activates the transcription factor c-Jun (Hibi et al., 1993). The phosphorylation of c-Jun was transiently increased in response to CAY treatment (Figure 4H). On the other hand, treatment with JNK inhibitor SP600125 prevented caspase-3/7 activation (Figure S5F) and reverted CAY-mediated cytotoxicity (Figure 4I). Additionally, the overexpression of a dominant-negative IRE1 (Tirasophon et al., 1998) (K599A) but not wild-type IRE1 produced significant rescue from cell death mediated by CAY or PA treatment (Figure S5G). Furthermore, treatment with two IRE1 inhibitors, 4μ8C (Cross et al., 2012) and KIRA6 (Ghosh et al., 2014), prevented caspase-3/7 activation (Figure S5F) and almost completely abrogated CAY-mediated cytotoxicity (Figures 4I, S5H, and S5I). The ATF6 inhibitor Ceapin A7 (Gallagher et al., 2016) failed to prevent cell death, while the PERK inhibitor GSK2656157 produced significant rescue from cell death in two of the three GSCs tested (Figures 4I, S5H, and S5I). It should be noted that both PERK and IRE1 have redundant functions and are able to switch from ER stress regulators to apoptosis effectors when ER homeostasis is unattainable (Han et al., 2009). Overall, SCD1 inhibition induces terminal UPR signaling and triggers apoptotic cell death via IRE1 and JNK.

Adaptive ER Stress Response Promotes SCD1 Expression through SREBP1 Activation

Given its cytoprotective properties, we asked whether SCD1 is transcriptionally activated under ER stress in order to support GSC survival. Tg-induced ER stress resulted in a

Figure 4. SCD1 Inhibition Promotes ER Stress and Triggers UPR-Mediated Apoptotic Signaling

(A) Relative mRNA expression of ER stress markers in GSCs treated with CAY (200 nM) for 24 and 48 h.

(B) Immunoblot analysis of four GSCs treated with CAY for 48 h.

(C) Fold change in caspase-3/7 activation after treatment with CAY (50 nM) in the presence or absence of PA (50 μM) or OA (50 μM).

(D) Cell viability in five GSC specimens and NHA, treated with CAY (50 nM) or the combination of CAY and PA (50 μM) for 4 days.

(E) Fold change in caspase-3/7 activation after treatment with CAY (50 nM) in the presence or absence of PBA (5 mM).

(F) Cell viability in GSCs pretreated with CAY for 24 h followed by PBA treatment for 4 days.

(G) Relative mRNA expression of *sXBP1* and *CHOP* in GSCs treated with CAY and/or OA (50 μM).

(H) Immunoblot analysis of phosphorylated c-Jun in GSCs treated with CAY.

(I) Cell viability of GSCs treated with CAY (50 nM) or the combination of CAY with: JNK inhibitor (SP 600125: 20 μM), IRE1 inhibitors (4μ8C: 25 μM and KIRA6: 5 μM), PERK inhibitor (GSK2656157: 10 μM), and ATF6 inhibitor (Ceapin A7: 20 μM).

See also Figures S4 and S5.

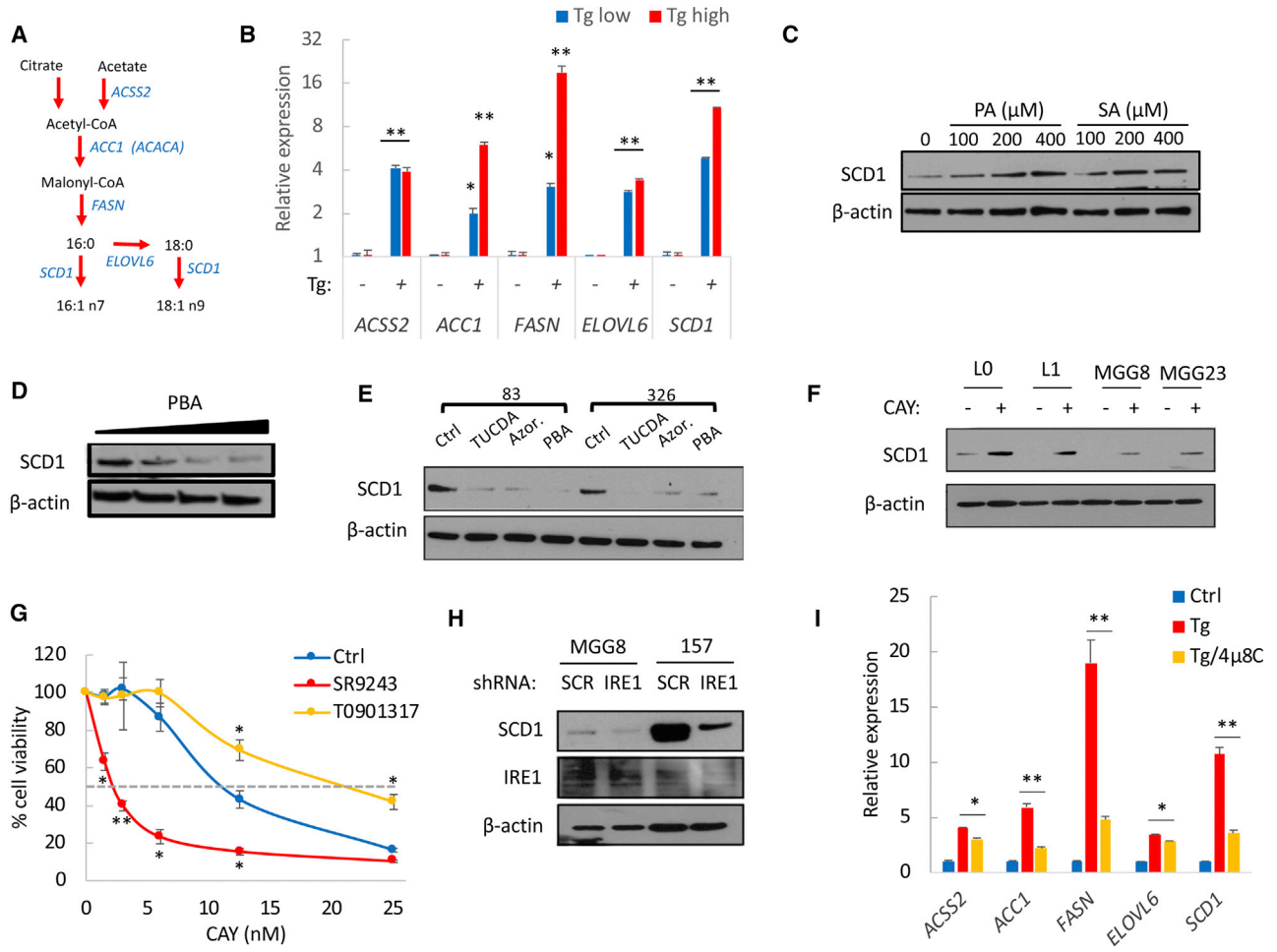

Figure 5. ER Stress Promotes a Lipogenic Signature through SREBP1 and IRE1 Signaling

(A) *De novo* lipogenesis pathway.

(B) Relative mRNA expression of SREBP1 target genes in GSCs treated with Tg (200 nM).

(C–E) Protein expression of SCD1 in GSCs treated with PA and SA (C) or the ER stress inhibitors PBA (2.5, 5, and 10 mM), TUCDA (0.5 mM), and azoramide (50 μM) (D and E).

(F) Immunoblot analysis showing an increased SCD1 expression in four GSCs treated with CAY (200 nM).

(G) Cell viability in GSCs treated with the indicated doses of CAY in combination with T0901317 (25 μM) or SR9243 (10 μM) for 3 days.

(H) Immunoblot analysis of SCD1 expression following IRE1 knockdown.

(I) Relative mRNA expression of SREBP1 target genes in GSCs treated with Tg (300 nM) in the presence or absence of IRE1 inhibitor 4μ8C.

*$p < 0.05$, **$p < 0.001$, Student's t test. See also Figures S6 and S7.

dose-dependent increase of SREBP1 transcriptional targets involved in *de novo* lipid synthesis including *SCD1*, *FASN*, *ACC1*, acyl-CoA synthetase short chain family member 2 (*ACSS2*), and ELOVL fatty acid elongase 6 (*ELOVL6*) (Figures 5A and 5B). Silencing of SREBP1 effectively decreased the expression of these genes (Figure S6A) and, concurrently with SCD1 downregulation, resulted in a strong decrease (>60%) in mRNA expression of stem cell markers (Figure S6B). Furthermore, the upregulation of SREBP1 target genes by Tg, confirmed in a second GSC specimen (Figure S6C), was reversed after SREBP1 silencing (data not shown) or concomitant treatment with 25-hydroxycholesterol (25-HC), an inhibitor of SREBP processing (Adams et al., 2004) (Figure S6C). ER stress-mediated increase of SCD1 protein expression was further confirmed after treatment with PA or SA (Figure 5C) or with the synthetic compound HA15, which triggers ER stress by specifically targeting BiP (Cerezo et al., 2016) (Figure S6D). Conversely, alleviating ER stress with PBA, azoramide, or tauroursodeoxycholic acid (TUCDA) downregulated SCD1 protein levels (Figures 5D and 5E). Thus, endogenous ER stress also contributes to SCD1 transcriptional regulation.

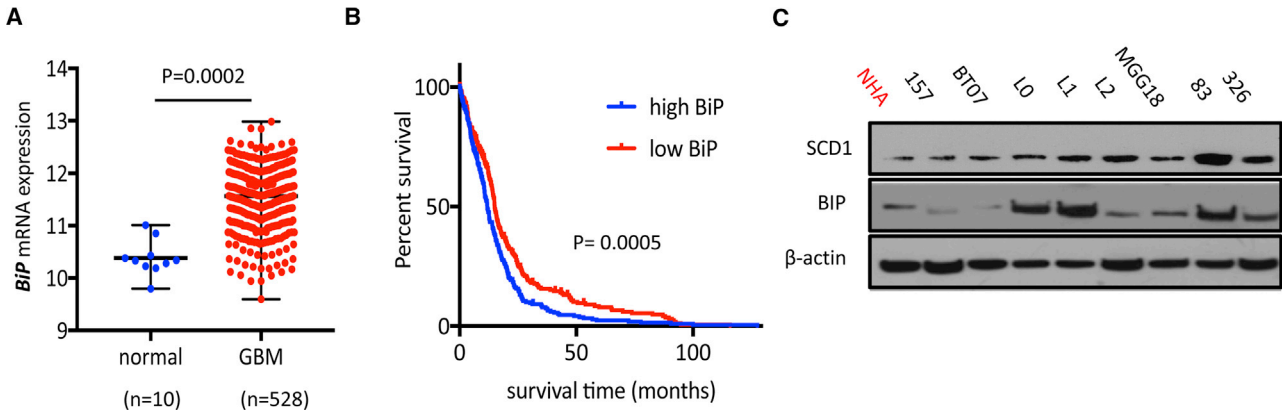

Figure 6. The Expression of BiP Is Increased in GBM and Predicts Sensitivity to SCD1 Inhibition

(A) TCGA analysis of *BiP* mRNA expression in normal non-tumor and GBM.

(B) Survival analysis in 525 GBM patients from the TCGA dataset based on high versus low *BiP* expression levels. p = 0.0005, log-rank test.

(C) Immunoblot analysis of SCD1 and BiP expression in NHA and eight GSC specimens.

See also Figure S7.

Intriguingly, due to the accumulation of SFAs, we observed an increased SCD1 expression following CAY treatment (Figure 5F). Blocking SCD1 transcriptional activation would prevent *de novo* synthesis of this desaturase and likely increase cytotoxicity of SCD1 inhibitors. Since the nuclear receptor liver-X-receptor (LXR) directly activates the expression of SREBP1, we used a selective LXR agonist T0901317, and an inverse agonist SR9243, to forcibly activate or repress LXR, respectively. The LXR inverse agonist effectively decreased SCD1 expression, which was increased after treatment with the LXR agonist (Figure S6E). Concomitant treatment with SR9243 and CAY further increased ER stress markers compared with the SCD1 inhibitor alone (Figure S6F). Unexpectedly, despite a strong downregulation of SCD1 by SR9243, the latter did not cause any significant increase in ER stress (Figure S6F) or cytotoxicity (Figure S6G). This is likely justified by the lack of SFA biosynthesis and accumulation after LXR inhibition. On the other hand, the combined treatment of SR9243 with low doses of CAY (<25 nM) decreased GSC viability (Figures 5G and S6H), while the LXR agonist T0901317 protected from CAY-mediated cell death (Figure 5G). Collectively, our data suggest that cytotoxicity caused by SCD1 inhibition is primarily due to toxic accumulation of SFAs. Therefore, targeting SCD1 and not upstream lipogenesis regulators is likely to achieve the best therapeutic outcome.

IRE1 Signaling Is Essential for Transcriptional Activation of *De Novo* Lipid Synthesis Genes

Given that sustained IRE1 activity promotes cell survival under ER stress, we asked whether IRE1 is an upstream regulator of SREBP1 transcriptional activity. The overexpression of IRE1 that is sufficient to activate IRE1 signaling increased *XBP1* splicing (Figure S7A) and upregulated SREBP1 target genes (Figure S7B). On the other hand, silencing of IRE1 resulted in a decreased expression of SREBP1 targets including *SCD1* (Figures 5H and S7C) and prevented their upregulation following Tg treatment (Figure S7C). Finally, concurrent treatment with Tg and the IRE1 inhibitor 4μ8C prevented *XBP1* splicing (Figure S7D) and essentially suppressed the upregulation of lipogenesis target genes (Figure 5I). Taken together, these results indicate that IRE1 controls the transcriptional activation of SREBP1 targets including SCD1.

The Expression of BiP Predicts Response to SCD1 Inhibition

Elevated expression of BiP, the putative marker of ER stress, is commonly observed in various malignancies including GBM (Pyrko et al., 2007). Analysis of The Cancer Genome Atlas (TCGA) database confirmed that *BiP* expression is significantly increased in GBM compared with non-tumor tissue (Figure 6A), and elevated levels of *BiP* correlated with poor survival (Figure 6B). Furthermore, concordant with an increased *SCD1* expression by ER stress, we observed a positive correlation between the transcriptional levels of *BiP* and *SCD1* in GBM patients using the TCGA datasets (Pearson's r = 0.2686; p < 0.0001; Figure S7E). We then compared SCD1 and BiP protein expression across different GSCs. Interestingly, we observed a strong correlation between high BiP expression and sensitivity to SCD1 inhibitors; all four GSCs (L0, L1, 83, and 326) that were highly responsive to CAY treatment (Figure 2E) presented the highest BiP protein expression (Figure 6C), suggesting that GSCs with elevated endogenous ER stress are more dependent on SCD1. This was confirmed in the FC population which, in addition to increased expression of SREBP1 targets

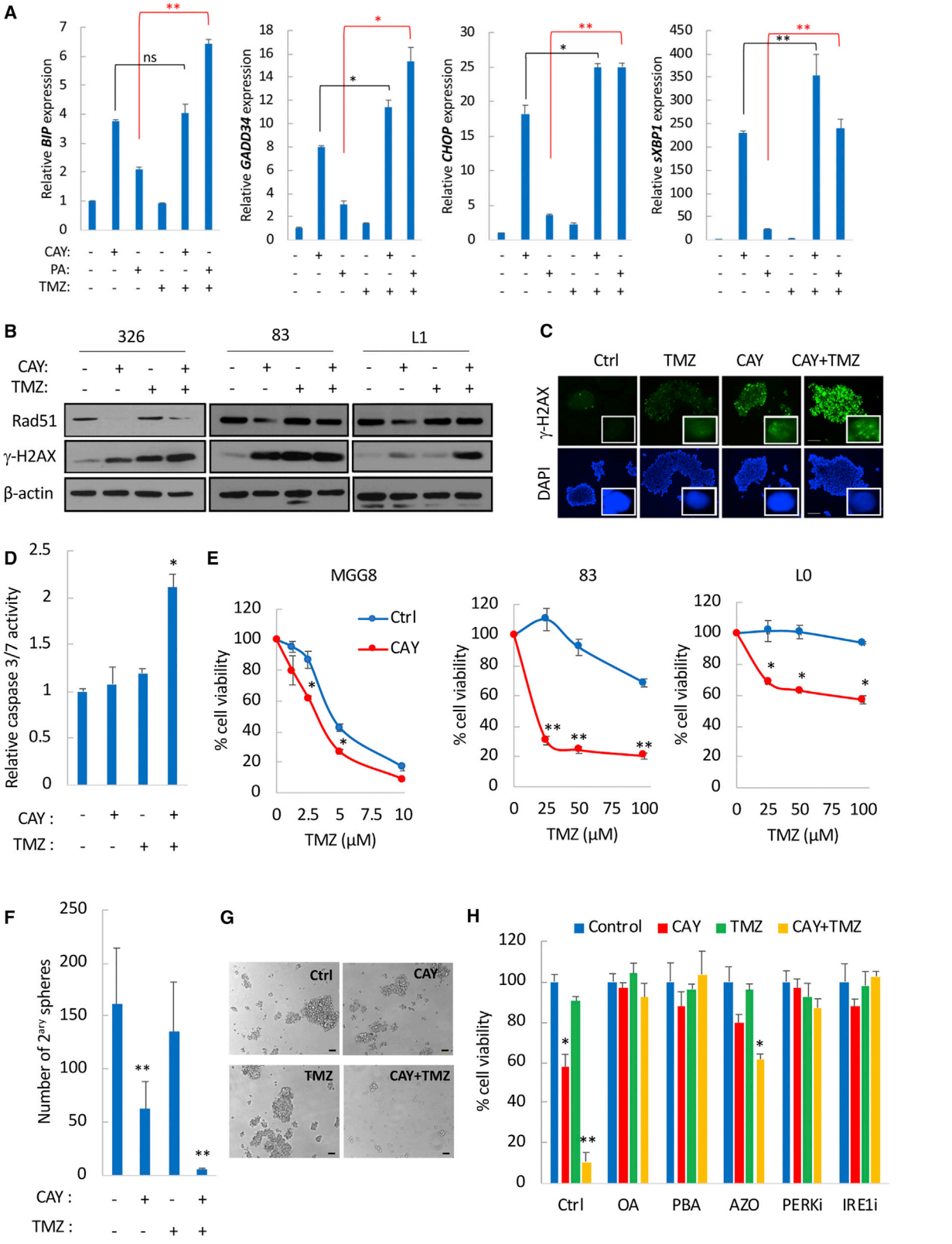

(legend on next page)

(Figure S1D), showed increased levels of ER stress markers compared with their parental neurospheres (Figures S7F and S7G). Additionally we initially reported that GSCs with mesenchymal properties are highly sensitive to short-term cytotoxicity of SCD1 inhibitors (Figure S1G). TCGA analysis of *BiP* and *CHOP*, across the three main GBM subtypes, shows that mesenchymal GBM expresses high levels of *BiP* and *CHOP* compared with proneural and classical subtypes (Figure S7H). Overall, GBM tumors with increased ER stress, which is often linked to an aggressive tumor behavior and poor prognosis, are increasingly vulnerable to SCD1 inhibition.

SCD1 Inhibition Downregulates DNA-Repair Mechanisms and Enhances Temozolomide Cytotoxicity

ER stress-inducing compounds can impair DNA-repair mechanisms and therefore sensitize to the conventional GBM therapeutic temozolomide (TMZ) (Weatherbee et al., 2016; Xipell et al., 2016), which in itself induces ER stress in GBM (Pyrko et al., 2007). Treatment of GSCs with TMZ resulted in a modest increase in mRNA expression of *CHOP* and *sXBP1* (<3-fold) (Figure 7A). The combination of CAY and TMZ displayed an overall increase in ER stress markers compared with CAY alone (Figure 7A). To assess whether this increase is caused by SFAs, we treated GSCs with TMZ and a relatively low dose of PA. Remarkably, the combination of TMZ with PA led to a prominent upregulation of all four markers (Figure 7A). Treatment with CAY in GSCs specimens consistently decreased the expression of the DNA-repair protein RAD51, which contributes to GSC resistance to radiation therapy and TMZ (Short et al., 2011) (Figure 7B). As such, treatment with CAY and TMZ resulted in increased levels of γ-H2AX (Figures 7B and 7C) and caspase-3/7 activation even in MGG23, a TMZ-resistant GSC with unmethylated MGMT promoter (Wakimoto et al., 2012) (Figure 7D). Importantly, treatment with CAY (10–100 nM) increased TMZ cytotoxicity in TMZ-responsive GSCs and sensitized to TMZ in TMZ-resistant GSCs (Figure 7E). For instance, in MGG23 this combination decreased cell viability by ~60% (Figure S7I) and depleted secondary sphere formation (Figures 7F and 7G). Treatment with PA (but not OA) also strongly sensitized to TMZ (Figures S7J and S7K). Finally, CAY-mediated sensitization to TMZ, which was confirmed in one additional GSC specimen (Figure 7H), could be completely reversed by alleviating ER stress or by inhibiting PERK or IRE1 (Figure 7H). Overall, these data indicate that ER stress induced by the accumulation of SFAs impairs RAD51-mediated DNA-repair mechanisms, thus sensitizing to TMZ.

DISCUSSION

Aberrant activation of UPR signaling is intimately associated with several hallmarks of cancer and is reported in different tumor types including GBM (Obacz et al., 2017). This high dependence on UPR signaling creates a vulnerability that could be exploited to target these tumors. In this study, we have identified an increased activation and dependence on SCD1 activity that is necessary for GSC maintenance and proliferation. IRE1 signaling typically promotes survival under low or moderate ER stress and contributes to GBM progression (Lhomond et al., 2018). However, under irremediable ER stress, IRE1 converts to a proapoptotic signaling (Han et al., 2009). Following a similar paradigm, we show that in GBM, IRE1 activation of SREBP1 transcriptional targets, which include SCD1, promotes survival under ER stress. While we have not addressed the mechanism by which IRE1 activates SREBP1, it was previously reported that sXBP1, a key transcription factor downstream of IRE1, can directly interact with SREBP1 promoter (Ning et al., 2011). Disruption of SCD1 activity in GSCs prevents synthesis of UFAs required for membrane synthesis and cell proliferation and causes a toxic accumulation of SFAs, thus leading to terminal UPR signaling mediated by JNK. In line with

Figure 7. SCD1 Inhibition Compromises DNA Damage Repair and Increases Temozolomide Cytotoxicity

(A) Relative mRNA expression of ER stress markers in 83-GSCs treated with CAY (200 nM), PA (200 μM), TMZ (100 μM), or their respective combination as indicated.

(B) Immunoblot analysis of Rad51 and γ-H2AX in GSCs treated with CAY and TMZ.

(C) Immunostaining for γ-H2AX in 83-GSCs treated with CAY (50 nM) and TMZ (100 μM). Scale bar, 200 μm. Representative images of single nuclei depicting γ-H2AX foci are also shown (inset).

(D) Fold change in caspase-3/7 activation in GSCs pretreated with CAY (200 nM) followed by TMZ treatment (100 μM).

(E) GSCs were pretreated with CAY for 24 h prior to TMZ treatment. Cell viability was measured after 5 days. MGG8 were treated with CAY (100 nM) and TMZ (0–10 μM). GSCs (83 and L0) were treated with CAY (10 nM) and TMZ (0–100 μM).

(F and G) MGG23 were pretreated with CAY (100 nM) for 24 h followed by TMZ (100 μM) for 7 days. Secondary spheres were counted 15 days after treatment (F). Micrographs of neurospheres are shown in (G). Scale bar, 100 μm.

(H) Cell viability in 326-GSCs after 7 days of treatment with CAY (10 nM), TMZ (50 μM), or their combination in the presence of OA, PBA, azoramide, PERK, or IRE1 inhibitor.

See also Figure S7.

our findings, SREBP1 and its target SCD1 were shown to be upregulated under hypoxic conditions in GBM (Lewis et al., 2015). This is possibly caused by IRE1 activation since hypoxia is known to activate the UPR, including IRE1-XBP1 signaling (Romero-Ramirez et al., 2004). Additionally, IRE1 activates downstream oncogenic signaling such as NF-κB (Cubillos-Ruiz et al., 2017), a regulator of SCD1 in ovarian cancer stem cells (Li et al., 2017). Therefore, it is likely that IRE1-mediated activation of SREBP1 targets is not limited to GBM. Our work also extends our previous findings whereby we have characterized a subpopulation of GBM stem cells with increased tumorigenic potential and aberrant activation of NF-κB (Teng et al., 2017). Interestingly, we have previously determined that these cells are enriched under acidic pH or hypoxia. Here, we provide mechanistic insights detailing an activated ER stress and SREBP1 signature as well as an increased vulnerability to SCD1 inhibition in these cells. Therefore, it is likely that IRE1-XBP1-NF-κB signaling is a key driver of aggressive GBM subpopulations.

An upregulation of SREBP1-mediated lipid synthesis is both a prerequisite and a consequence of the increased proliferation of tumor cells, potentially fueled by the biochemical environment of GBM, or endogenously by oncogenic stress, genomic instability, or misfolded proteins, all of which promote ER stress and UPR signaling. ER stress is further compounded by an avid uptake of free SFAs such as PA, the most abundant SFA in human serum and in most diets. Based on our mechanistic findings, and given its cytoprotective function, we propose that SCD1 activation is a metabolic adaptation by tumor cells to mitigate cellular damage under prolonged ER stress. This, in addition to its critical role in UFA synthesis essential for tumor cell proliferation and signaling, creates a "non-oncogene addiction" to SCD1 activity in GBM.

Prominent ER stress characterized by elevated expression of BiP renders GBM cells highly susceptible to SCD1 inhibition. An increased expression of BiP is commonly observed in cancer and correlates with chemoresistance (Luo and Lee, 2013; Roller and Maddalo, 2013). Since the upregulation of SCD1 is part of the cellular adaptation to ER stress, and SCD1 expression promotes self-renewal and tumor growth, increased SCD1 expression is de facto linked to therapeutic resistance. Indeed, SCD1 was found to be upregulated in TMZ-resistant GBM cell lines, and this upregulation reportedly promotes resistance to TMZ through the activation of AKT signaling (Dai et al., 2017). ER stress can affect genomic stability and DNA-repair mechanisms (Chevet et al., 2015). SCD1 inhibition resulted in increased DNA damage. Furthermore, the UPR triggers aberrant proteasomal degradation of proteins, a process referred to as ER-associated degradation (Travers et al., 2000). Accordingly, we propose an alternative mechanism of TMZ sensitization in GSCs with impaired SCD1 activity, primarily driven by overwhelming ER stress and the ensuing UPR-mediated degradation of RAD51.

Our study provides a proof of concept that effective pharmacological targeting of SCD1 achieves a strong therapeutic outcome, since intranasal delivery of CAY at relatively low doses significantly improved overall survival in one GSCs xenograft mouse model and completely prevented tumor growth with a 100% cure rate in a second model. This strong *in vivo* therapeutic outcome is likely attributed to a heightened ER stress and therefore increased vulnerability to SCD1 inhibition in the tumor environment. While this outcome is very promising, there are significant challenges that remain pertinent. One key question is the ideal delivery route of such inhibitors in humans in a way to maximize brain tumor penetrance and minimize systemic toxicity. We propose that delivery of therapeutics such as SCD1 inhibitors through nasal instillation warrants careful consideration and should be evaluated. This technique has several advantages, chief among which is its ability to bypass the blood-brain barrier (Chauhan and Chauhan, 2015) and minimize systemic toxicity due to rapid delivery of molecules directly to the brain. For clinical evaluation of such therapy, target engagement and effectiveness of SCD1 inhibitors could be evaluated in patients through *in vivo* proton magnetic resonance spectroscopy, which can readily detect lipid peaks and predominantly those corresponding to UFAs (Griffin et al., 2003).

Our *in vivo* results strongly suggest that free UFAs cannot circumvent or protect from SCD1 inhibition. It should be noted that all experimental animals were fed *ad libitum* with a chow diet, which contains a significant amount of fatty acids, in particular OA. Furthermore, we argue that the overwhelming cytotoxicity caused by SCD1 inhibition is due to toxic accumulation of SFAs in the tumor and ensuing ER stress. Based on our results, targeting of SCD1, but not general regulators of lipogenesis (SREBP1, LXR) or other *de novo* lipogenesis enzymes upstream of SCD1, is likely to be most effective because of the resulting accumulation of SFAs.

Taken together, our findings reveal that SCD1 activity provides a survival advantage for GBM cancer stem cells, which presents a metabolic vulnerability to SCD1 inhibition. We provide preclinical evidence that effective targeting of this enzyme can achieve a robust therapeutic outcome for this incurable brain cancer.

EXPERIMENTAL PROCEDURES

Cell-Based Assays

CellTiter-Glo (Promega) was used to measure cell viability. CellTiter 96 Aqueous One Solution (Promega) was used to measure cell proliferation. Caspase-3/7 activity was detected using Caspase-Glo 3/7 (Promega). All reagents were used as recommended

by the manufacturer. For data analysis, each data point in the treated samples was normalized to its respective vehicle or pretreatment control. Detailed methods for different experiments can be found in the Supplemental Information.

Immunoblot Analysis

Cells were lysed in RIPA buffer (Boston Bio Products) supplemented with protease and phosphatase inhibitors. Proteins were quantified using the Bradford protein determination assay (Bio-Rad), and 20–30 μg of protein were loaded and resolved on 10% NuPAGE Bis-Tris gels (Life Technologies) then transferred to nitrocellulose membranes (Bio-Rad) before incubation with the indicated antibodies. Proteins were detected using SuperSignal West Pico Chemiluminescent Substrate (Pierce).

Immunocytochemistry

Cells grown as neurospheres were fixed with ice-cold acetone for 20 min. Cells were mounted on slides, air dried, permeabilized with 0.1% Triton X-100, and simultaneously blocked with 5% BSA for 1 h at room temperature. Cells were incubated overnight at 4°C with γ-H2AX antibody (1:400) or SOX2 and NESTIN antibodies (1:100). Fluorophore-conjugated secondary antibodies (Life Technologies, 1:100) were then added and incubated for 1 h. Cell nuclei were counterstained with DAPI (Life Technologies), mounted on a microscope slide, and analyzed by fluorescence microscopy.

Mouse Orthotopic Brain Tumor Models

All animal studies were approved by the Massachusetts General Hospital Subcommittee on Research Animal Care and complied with guidelines set forth by the NIH Guide for the Case and Use of Laboratory Animals. GSCs (at the indicated dose) expressing Firefly luciferase (Fluc) were stereotactically implanted into the left forebrain of nude mice (2.5 mm lateral and 0.5 mm anterior to bregma, at a 2.5-mm depth from the skull surface). Tumor initiation and growth were monitored by imaging Fluc bioluminescence activity using a Xenogen IVIS 200 Imaging System (PerkinElmer), after intraperitoneal (i.p.) injections of D-luciferin (150 mg/kg body weight) (Gold Biotechnology). Image intensity was quantitated using the Living Image software 4.3.1 (PerkinElmer). CAY was delivered by topical instillation in the nose; this compound was initially dissolved in DMSO (100 mM). CAY was freshly resuspended in a 20% solution of (2-hydroxypropyl)-β-cyclodextrin (Sigma) and injected dropwise intranasally (final volume 20 μL). PA was delivered by i.p. injections.

Histological Analysis

Brains were collected following euthanasia, fixed in 4% paraformaldehyde, and cryoprotected in sucrose solution. Brain sections were prepared from fresh-frozen brain and subjected to H&E, BODIPY 493/503 (Thermo Fisher), or Ki67 staining according to standard protocols.

Statistical Analysis

All cell culture experiments (with the exception of fatty acid analyses, which were performed in one replicate) consisted of a minimum of three independent replicates and were repeated at least three times. Statistical significance was calculated using a two-tailed Student's t test, and p values of 0.05 or less were considered significant. The results are presented as the mean ± SD. Experiments involving animal survival were analyzed using a log-rank (Mantel-Cox) test and plotted as Kaplan-Meier survival curves using GraphPad Prism. Group size was solely determined based on preliminary tests, and no statistical method was used to determine sample size.

SUPPLEMENTAL INFORMATION

Supplemental Information can be found online at https://doi.org/10.1016/j.stemcr.2019.02.012.

AUTHOR CONTRIBUTIONS

Conceptualization, C.E.B.; Methodology, A.K.I and C.E.B.; Investigation, K.P., D.J.P., A.H., A.B.K., I.A., K.R., C.C.d.H., J.T., P.S.C., L.C., G.G.-I., A.K., and C.E.B.; Writing – Original Draft, K.P., D.J.P., and C.E.B. Writing – Review & Editing, K.P., D.J.P., and C.E.B.; Visualization: C.E.B.; Funding Acquisition, C.E.B.; Resources, C.E.B.; Supervision, C.E.B.

ACKNOWLEDGMENTS

We are very grateful to Drs. Hiroaki Wakimoto (MGH), Ichiro Nakano (University of Alabama Birmingham) and Brent Reynolds (University of Florida) for providing primary GBM cells; Dr. Peter Walter (USCF/HHMI) for providing Ceapin A7; Dr. Bakhos Tannous for critical reading of the manuscript; and Dr. Anders Naar for helpful discussion and input. We also thank Dr. Luzia Sampaio and Mohamed El-Abtah for technical assistance. We acknowledge the MGH Vector Core supported by NIH/NINDS P30NS04776 and 1S10RR025504 Shared Instrumentation grant for the IVIS imaging system. This work was supported by the NIH, NCI grant K22CA197053 (to C.E.B.)

Received: January 8, 2019
Revised: February 23, 2019
Accepted: February 26, 2019
Published: March 28, 2019

REFERENCES

Adams, C.M., Reitz, J., De Brabander, J.K., Feramisco, J.D., Li, L., Brown, M.S., and Goldstein, J.L. (2004). Cholesterol and 25-hydroxycholesterol inhibit activation of SREBPs by different mechanisms, both involving SCAP and Insigs. J. Biol. Chem. *279*, 52772–52780.

Carta, G., Murru, E., Banni, S., and Manca, C. (2017). Palmitic acid: physiological role, metabolism and nutritional implications. Front. Physiol. *8*, 902.

Cerezo, M., Lehraiki, A., Millet, A., Rouaud, F., Plaisant, M., Jaune, E., Botton, T., Ronco, C., Abbe, P., Amdouni, H., et al. (2016). Compounds triggering ER stress exert anti-melanoma effects and overcome BRAF inhibitor resistance. Cancer Cell *29*, 805–819.

Chauhan, M.B., and Chauhan, N.B. (2015). Brain uptake of neurotherapeutics after intranasal versus intraperitoneal delivery

in mice. J. Neurol. Neurosurg. *2*. https://doi.org/10.19104/jnn.2015.91.

Chevet, E., Hetz, C., and Samali, A. (2015). Endoplasmic reticulum stress-activated cell reprogramming in oncogenesis. Cancer Discov. *5*, 586–597.

Cross, B.C., Bond, P.J., Sadowski, P.G., Jha, B.K., Zak, J., Goodman, J.M., Silverman, R.H., Neubert, T.A., Baxendale, I.R., Ron, D., and Harding, H.P. (2012). The molecular basis for selective inhibition of unconventional mRNA splicing by an IRE1-binding small molecule. Proc. Natl. Acad. Sci. U S A *109*, E869–E878.

Cubillos-Ruiz, J.R., Bettigole, S.E., and Glimcher, L.H. (2017). Tumorigenic and immunosuppressive effects of endoplasmic reticulum stress in cancer. Cell *168*, 692–706.

Dai, S., Yan, Y., Xu, Z., Zeng, S., Qian, L., Huo, L., Li, X., Sun, L., and Gong, Z. (2017). SCD1 confers temozolomide resistance to human glioma cells via the Akt/GSK3beta/beta-catenin signaling axis. Front. Pharmacol. *8*, 960.

Fu, S., Yalcin, A., Lee, G.Y., Li, P., Fan, J., Arruda, A.P., Pers, B.M., Yilmaz, M., Eguchi, K., and Hotamisligil, G.S. (2015). Phenotypic assays identify azoramide as a small-molecule modulator of the unfolded protein response with antidiabetic activity. Sci. Transl. Med. *7*, 292ra298.

Gallagher, C.M., Garri, C., Cain, E.L., Ang, K.K., Wilson, C.G., Chen, S., Hearn, B.R., Jaishankar, P., Aranda-Diaz, A., Arkin, M.R., et al. (2016). Ceapins are a new class of unfolded protein response inhibitors, selectively targeting the ATF6alpha branch. Elife *5*. https://doi.org/10.7554/eLife.11878.

Ghosh, R., Wang, L., Wang, E.S., Perera, B.G., Igbaria, A., Morita, S., Prado, K., Thamsen, M., Caswell, D., Macias, H., et al. (2014). Allosteric inhibition of the IRE1alpha RNase preserves cell viability and function during endoplasmic reticulum stress. Cell *158*, 534–548.

Griffin, J.L., Lehtimaki, K.K., Valonen, P.K., Grohn, O.H., Kettunen, M.I., Yla-Herttuala, S., Pitkanen, A., Nicholson, J.K., and Kauppinen, R.A. (2003). Assignment of ^{1}H nuclear magnetic resonance visible polyunsaturated fatty acids in BT4C gliomas undergoing ganciclovir-thymidine kinase gene therapy-induced programmed cell death. Cancer Res. *63*, 3195–3201.

Guo, D., Prins, R.M., Dang, J., Kuga, D., Iwanami, A., Soto, H., Lin, K.Y., Huang, T.T., Akhavan, D., Hock, M.B., et al. (2009). EGFR signaling through an Akt-SREBP-1-dependent, rapamycin-resistant pathway sensitizes glioblastomas to antilipogenic therapy. Sci. Signal. *2*, ra82.

Han, D., Lerner, A.G., Vande Walle, L., Upton, J.P., Xu, W., Hagen, A., Backes, B.J., Oakes, S.A., and Papa, F.R. (2009). IRE1alpha kinase activation modes control alternate endoribonuclease outputs to determine divergent cell fates. Cell *138*, 562–575.

Hibi, M., Lin, A., Smeal, T., Minden, A., and Karin, M. (1993). Identification of an oncoprotein- and UV-responsive protein kinase that binds and potentiates the c-Jun activation domain. Genes Dev. *7*, 2135–2148.

Igal, R.A. (2010). Stearoyl-CoA desaturase-1: a novel key player in the mechanisms of cell proliferation, programmed cell death and transformation to cancer. Carcinogenesis *31*, 1509–1515.

Lathia, J.D., Mack, S.C., Mulkearns-Hubert, E.E., Valentim, C.L., and Rich, J.N. (2015). Cancer stem cells in glioblastoma. Genes Dev. *29*, 1203–1217.

Lewis, C.A., Brault, C., Peck, B., Bensaad, K., Griffiths, B., Mitter, R., Chakravarty, P., East, P., Dankworth, B., Alibhai, D., et al. (2015). SREBP maintains lipid biosynthesis and viability of cancer cells under lipid- and oxygen-deprived conditions and defines a gene signature associated with poor survival in glioblastoma multiforme. Oncogene *34*, 5128–5140.

Lhomond, S., Avril, T., Dejeans, N., Voutetakis, K., Doultsinos, D., McMahon, M., Pineau, R., Obacz, J., Papadodima, O., Jouan, F., et al. (2018). Dual IRE1 RNase functions dictate glioblastoma development. EMBO Mol. Med. *10*. https://doi.org/10.15252/emmm.201707929.

Li, J., Condello, S., Thomes-Pepin, J., Ma, X., Xia, Y., Hurley, T.D., Matei, D., and Cheng, J.X. (2017). Lipid desaturation is a metabolic marker and therapeutic target of ovarian cancer stem cells. Cell Stem Cell *20*, 303–314.e5.

Luo, B., and Lee, A.S. (2013). The critical roles of endoplasmic reticulum chaperones and unfolded protein response in tumorigenesis and anticancer therapies. Oncogene *32*, 805–818.

Mao, P., Joshi, K., Li, J., Kim, S.H., Li, P., Santana-Santos, L., Luthra, S., Chandran, U.R., Benos, P.V., Smith, L., et al. (2013). Mesenchymal glioma stem cells are maintained by activated glycolytic metabolism involving aldehyde dehydrogenase 1A3. Proc. Natl. Acad. Sci. U S A *110*, 8644–8649.

Mason, P., Liang, B., Li, L., Fremgen, T., Murphy, E., Quinn, A., Madden, S.L., Biemann, H.P., Wang, B., Cohen, A., et al. (2012). SCD1 inhibition causes cancer cell death by depleting mono-unsaturated fatty acids. PLoS One *7*, e33823.

Ning, J., Hong, T., Ward, A., Pi, J., Liu, Z., Liu, H.Y., and Cao, W. (2011). Constitutive role for IRE1alpha-XBP1 signaling pathway in the insulin-mediated hepatic lipogenic program. Endocrinology *152*, 2247–2255.

Noto, A., Raffa, S., De Vitis, C., Roscilli, G., Malpicci, D., Coluccia, P., Di Napoli, A., Ricci, A., Giovagnoli, M.R., Aurisicchio, L., et al. (2013). Stearoyl-CoA desaturase-1 is a key factor for lung cancer-initiating cells. Cell Death Dis. *4*, e947.

Obacz, J., Avril, T., Le Reste, P.J., Urra, H., Quillien, V., Hetz, C., and Chevet, E. (2017). Endoplasmic reticulum proteostasis in glioblastoma—from molecular mechanisms to therapeutic perspectives. Sci. Signal. *10*. https://doi.org/10.1126/scisignal.aal2323.

Ostrom, Q.T., Gittleman, H., de Blank, P.M., Finlay, J.L., Gurney, J.G., McKean-Cowdin, R., Stearns, D.S., Wolff, J.E., Liu, M., et al. (2016). American brain tumor association adolescent and young adult primary brain and central nervous system tumors diagnosed in the United States in 2008-2012. Neuro Oncol. *18* (*Suppl 1*), i1–i50.

Pyrko, P., Schonthal, A.H., Hofman, F.M., Chen, T.C., and Lee, A.S. (2007). The unfolded protein response regulator GRP78/BiP as a novel target for increasing chemosensitivity in malignant gliomas. Cancer Res. *67*, 9809–9816.

Roller, C., and Maddalo, D. (2013). The molecular chaperone GRP78/BiP in the development of chemoresistance: mechanism and possible treatment. Front. Pharmacol. *4*, 10.

Rome, S., Lecomte, V., Meugnier, E., Rieusset, J., Debard, C., Euthine, V., Vidal, H., and Lefai, E. (2008). Microarray analyses of SREBP-1a and SREBP-1c target genes identify new regulatory pathways in muscle. Physiol. Genomics *34*, 327–337.

Romero-Ramirez, L., Cao, H., Nelson, D., Hammond, E., Lee, A.H., Yoshida, H., Mori, K., Glimcher, L.H., Denko, N.C., Giaccia, A.J., et al. (2004). XBP1 is essential for survival under hypoxic conditions and is required for tumor growth. Cancer Res. *64*, 5943–5947.

Ron, D., and Walter, P. (2007). Signal integration in the endoplasmic reticulum unfolded protein response. Nat. Rev. Mol. Cell Biol. *8*, 519–529.

Short, S.C., Giampieri, S., Worku, M., Alcaide-German, M., Sioftanos, G., Bourne, S., Lio, K.I., Shaked-Rabi, M., and Martindale, C. (2011). Rad51 inhibition is an effective means of targeting DNA repair in glioma models and CD133+ tumor-derived cells. Neuro Oncol. *13*, 487–499.

Srivastava, N.K., Pradhan, S., Gowda, G.A., and Kumar, R. (2010). In vitro, high-resolution ^{1}H and ^{31}P NMR based analysis of the lipid components in the tissue, serum, and CSF of the patients with primary brain tumors: one possible diagnostic view. NMR Biomed. *23*, 113–122.

Szegezdi, E., Logue, S.E., Gorman, A.M., and Samali, A. (2006). Mediators of endoplasmic reticulum stress-induced apoptosis. EMBO Rep. *7*, 880–885.

Tateishi, K., Iafrate, A.J., Ho, Q., Curry, W.T., Batchelor, T.T., Flaherty, K.T., Onozato, M.L., Lelic, N., Sundaram, S., Cahill, D.P., et al. (2016). Myc-driven glycolysis is a therapeutic target in glioblastoma. Clin. Cancer Res. *22*, 4452–4465.

Teng, J., Carla da Hora, C., Kantar, R.S., Nakano, I., Wakimoto, H., Batchelor, T.T., Chiocca, E.A., Badr, C.E., and Tannous, B.A. (2017). Dissecting inherent intratumor heterogeneity in patient-derived glioblastoma culture models. Neuro Oncol. *19*, 820–832.

Tirasophon, W., Welihinda, A.A., and Kaufman, R.J. (1998). A stress response pathway from the endoplasmic reticulum to the nucleus requires a novel bifunctional protein kinase/endoribonuclease (Ire1p) in mammalian cells. Genes Dev. *12*, 1812–1824.

Travers, K.J., Patil, C.K., Wodicka, L., Lockhart, D.J., Weissman, J.S., and Walter, P. (2000). Functional and genomic analyses reveal an essential coordination between the unfolded protein response and ER-associated degradation. Cell *101*, 249–258.

Urra, H., Dufey, E., Avril, T., Chevet, E., and Hetz, C. (2016). Endoplasmic reticulum stress and the hallmarks of cancer. Trends Cancer *2*, 252–262.

Volmer, R., van der Ploeg, K., and Ron, D. (2013). Membrane lipid saturation activates endoplasmic reticulum unfolded protein response transducers through their transmembrane domains. Proc. Natl. Acad. Sci. U S A *110*, 4628–4633.

Wakimoto, H., Mohapatra, G., Kanai, R., Curry, W.T., Jr., Yip, S., Nitta, M., Patel, A.P., Barnard, Z.R., Stemmer-Rachamimov, A.O., Louis, D.N., et al. (2012). Maintenance of primary tumor phenotype and genotype in glioblastoma stem cells. Neuro Oncol. *14*, 132–144.

Wang, M., and Kaufman, R.J. (2014). The impact of the endoplasmic reticulum protein-folding environment on cancer development. Nat. Rev. Cancer *14*, 581–597.

Weatherbee, J.L., Kraus, J.L., and Ross, A.H. (2016). ER stress in temozolomide-treated glioblastomas interferes with DNA repair and induces apoptosis. Oncotarget *7*, 43820–43834.

Xipell, E., Aragon, T., Martinez-Velez, N., Vera, B., Idoate, M.A., Martinez-Irujo, J.J., Garzon, A.G., Gonzalez-Huarriz, M., Acanda, A.M., Jones, C., et al. (2016). Endoplasmic reticulum stress-inducing drugs sensitize glioma cells to temozolomide through downregulation of MGMT, MPG, and Rad51. Neuro Oncol. *18*, 1109–1119.

Stem Cell Reports, Volume *12*

Supplemental Information

Stearoyl CoA Desaturase Is Essential for Regulation of Endoplasmic Reticulum Homeostasis and Tumor Growth in Glioblastoma Cancer Stem Cells

Kelsey Pinkham, David Jaehyun Park, Arsalan Hashemiaghdam, Aleksandar B. Kirov, Isam Adam, Kamila Rosiak, Cintia C. da Hora, Jian Teng, Pike See Cheah, Litia Carvalho, Gitali Ganguli-Indra, Avalon Kelly, Arup K. Indra, and Christian E. Badr

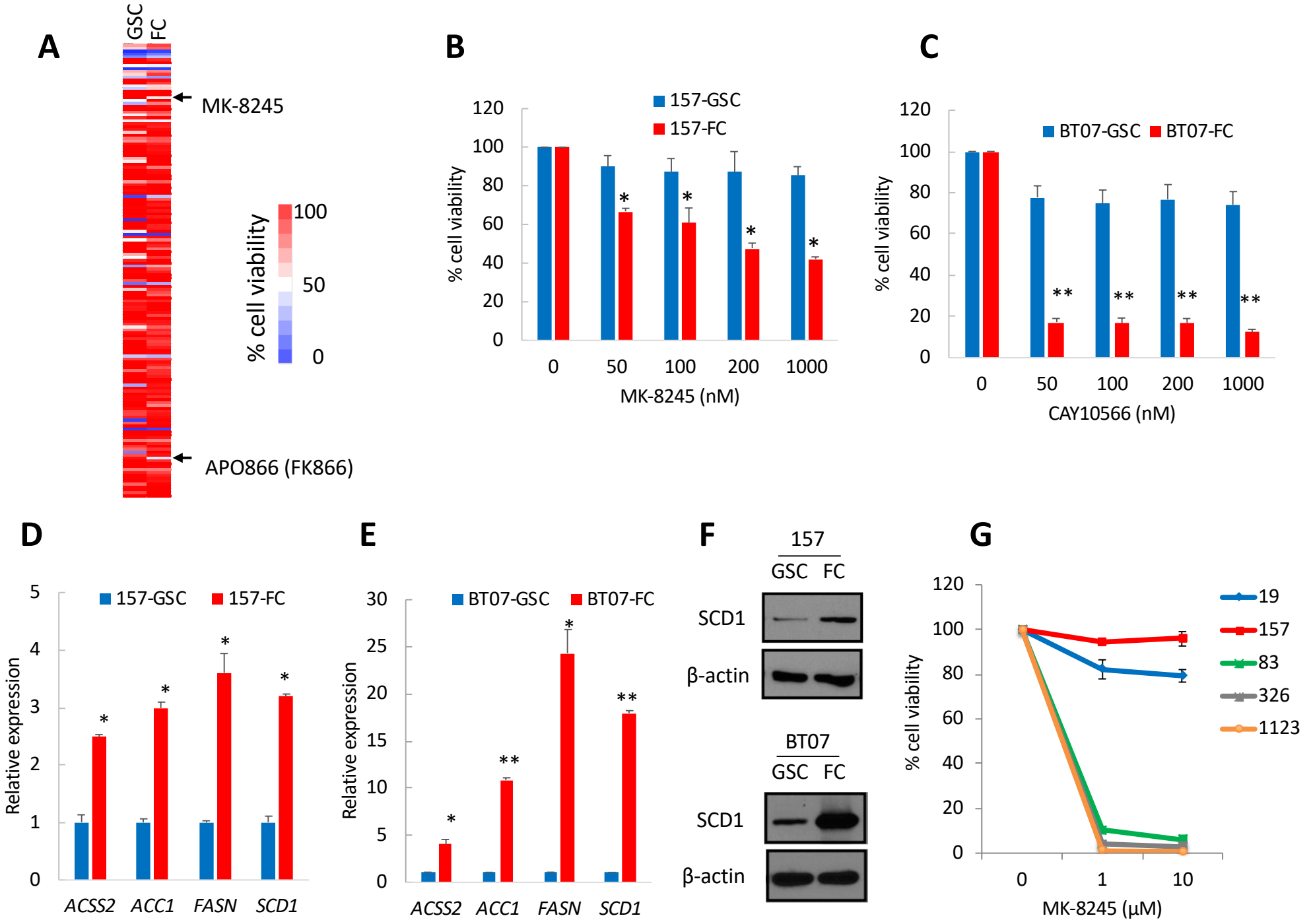
A
GSC
FC
MK-8245
APO866 (FK866)
% cell viability
100
50
0
B
157-GSC
157-FC
% cell viability
MK-8245 (nM)
0
50
100
200
1000
C
BT07-GSC
BT07-FC
% cell viability
CAY10566 (nM)
D
157-GSC
157-FC
Relative expression
ACSS2
ACC1
FASN
SCD1
E
BT07-GSC
BT07-FC
Relative expression
F
157
GSC
FC
SCD1
β-actin
BT07
G
% cell viability
MK-8245 (μM)
19
157
83
326
1123

Figure S1: SCD1 is a therapeutic target in highly proliferative GSC populations. Related to first paragraph in Results section. **A.** Targeted inhibitors screening in MGG23-GSCs and MGG23-FC. Heat map representing cell viability expressed at % of DMSO treated control, measured after 3 days of treatment. As shown, only two inhibitors for SCD1 (MK-8245) and NAMPT (APO866) resulted in increased cell death in FC compared to the parental GSCs. **B-C.** Two GSCs (157 and BT07) and their matching FC were treated with different doses of the indicated SCD1 inhibitors. Cell viability was measured 5 days after treatment. **D-E.** Relative mRNA expression of the indicated SREBP1 target genes in 157 and BT07 GSCs and their matching FC. **F.** Protein expression of SCD1 in 157 and BT07 GSCs and FC. **G.** Cell viability in proneural GSCs (19;157) and mesenchymal GSCs (83; 326; 1123) treated with MK-8245 for 4 days. *$p<0.05$; **$p<0.001$; Student t-test.

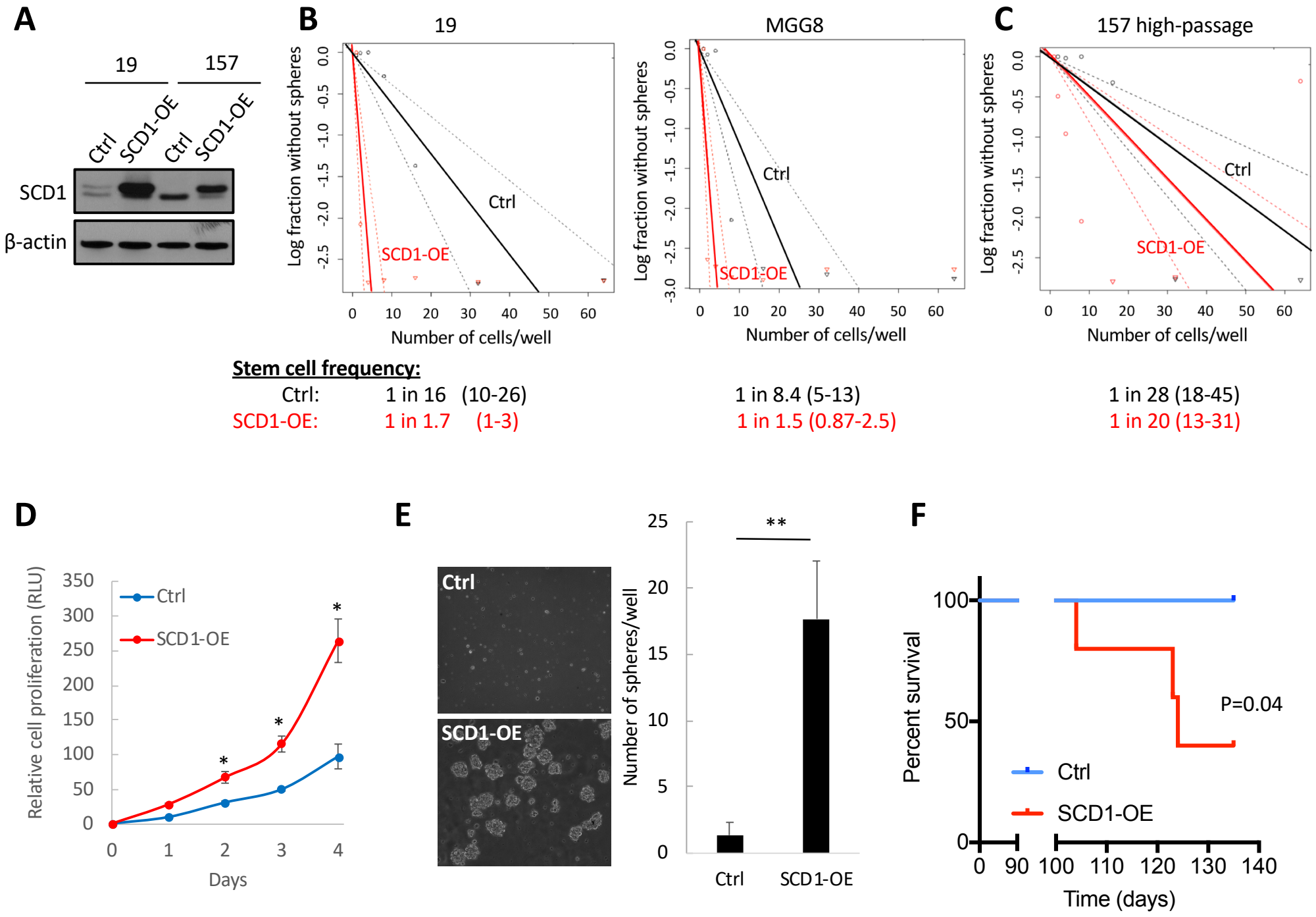
A
19
157
Ctrl
SCD1-OE
Ctrl
SCD1-OE
SCD1
β-actin
B
19
MGG8
C
157 high-passage
Log fraction without spheres
Number of cells/well
Ctrl
SCD1-OE
Stem cell frequency:
Ctrl: 1 in 16 (10-26) 1 in 8.4 (5-13) 1 in 28 (18-45)
SCD1-OE: 1 in 1.7 (1-3) 1 in 1.5 (0.87-2.5) 1 in 20 (13-31)
D
Relative cell proliferation (RLU)
Days
Ctrl
SCD1-OE
E
Number of spheres/well
**
F
Percent survival
Time (days)
P=0.04

Figure S2: SCD1 is essential for GSC maintenance and tumor initiation. Related to Figure 1. **A.** Immunoblot showing upregulated expression of SCD1 after transduction of two GSCs with lentivirus control or SCD1-OE. **B-C** Stem cell frequency in 19 and MGG8 GSCs (A) or high-passage 157 GSCs (B) transduced with control (Ctrl) or SCD1-expressing lentivirus (SCD1-OE) determined using the limited dilution analysis algorithm. **D.** Cell proliferation in high-passage 157 GSCs expressing Ctrl or SCD1-OE. **E.** The same cells were dissociated into single cells and plated at a density of 1 cell/µl. Secondary spheres were counted after 10 days. **F.** High-passage 157-Fluc GSCs ($5x10^4$) expressing a control lentivirus (Ctrl) or SCD1 (SCD1-OE) were implanted in the brain of nude mice (n=5/group). Kaplan-Meier curves showing median survival in both groups. (P values, two-sided log-rank test). *$p<0.05$; **$p<0.001$; Student t-test.

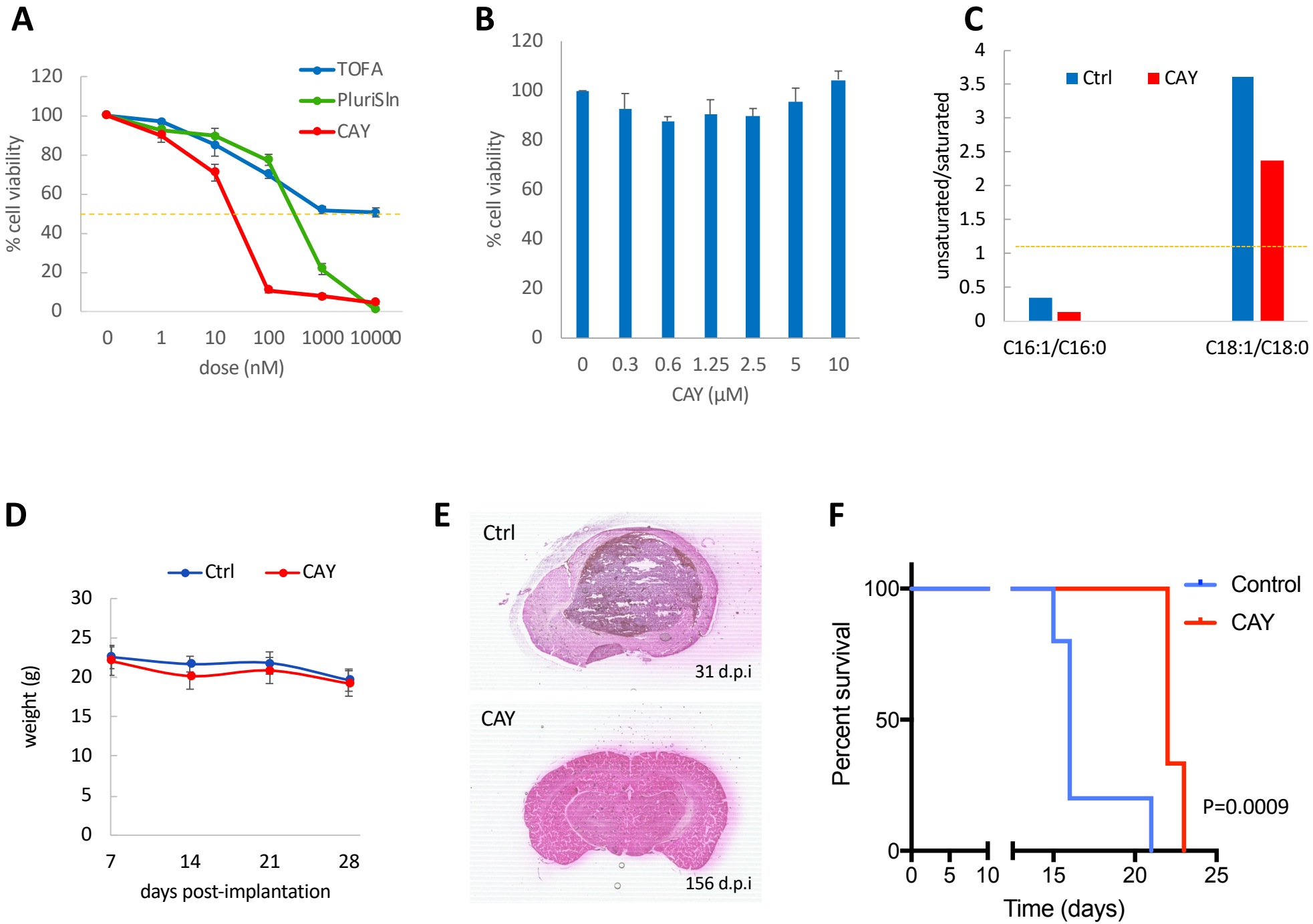
A
120
100
80
60
40
20
0
% cell viability
TOFA
PluriSln
CAY
0
1
10
100
1000
10000
dose (nM)
B
120
100
80
60
40
20
0
% cell viability
0
0.3
0.6
1.25
2.5
5
10
CAY (µM)
C
4
3.5
3
2.5
2
1.5
1
0.5
0
unsaturated/saturated
Ctrl
CAY
C16:1/C16:0
C18:1/C18:0
D
Ctrl
CAY
30
25
20
15
10
5
0
weight (g)
7
14
21
28
days post-implantation
E
Ctrl
31 d.p.i
CAY
156 d.p.i
F
100
50
0
Percent survival
Control
CAY
P=0.0009
0
5
10
15
20
25
Time (days)

Figure S3: Pharmacological targeting of SCD1. Related to Figures 2 and 3. **A.** GSCs were treated with the indicated inhibitors. Cell viability was measured 4 days after treatment. **B.** Cell viability in NHA treated with CAY in serum-free medium at the indicated doses for 4 days. **C.** Ratios of C16:1/C16:0 and C18:1/C18:0 in GSCs treated with CAY (200nM) for 48h. This comparison shows an abundance of C18:1 as compared to C16:1 prior to CAY treatment (since C18:1/C18:0 >1) and depicts a decrease in unsaturated fatty acids (C16:1 and C18:1) after treatment. **D.** Average weight of mice from Control and CAY-treated groups during and post-treatment shows no significant change. **E.** Brains from mice from the control group were isolated at day 25-31 post-implantation (dpi). Similarly brains of the 2 remaining mice from the CAY treated group were isolated at day 156 post-implantation. Brain sections were analyzed by H&E staining. Micrographs from one representative mouse per group are shown. **F.** Mice bearing 83-Fluc tumors (n=5/group) were treated with Ctrl (n=5) or CAY (n=6; 1.5 mg/kg) for 14 days starting at day 6 after implantation. Kaplan-Meier curves showing median survival for Control (16 days) and CAY10566 treated mice (22 days) with P=0.009; two-sided log-rank test. *$p<0.05$; Student t-test.

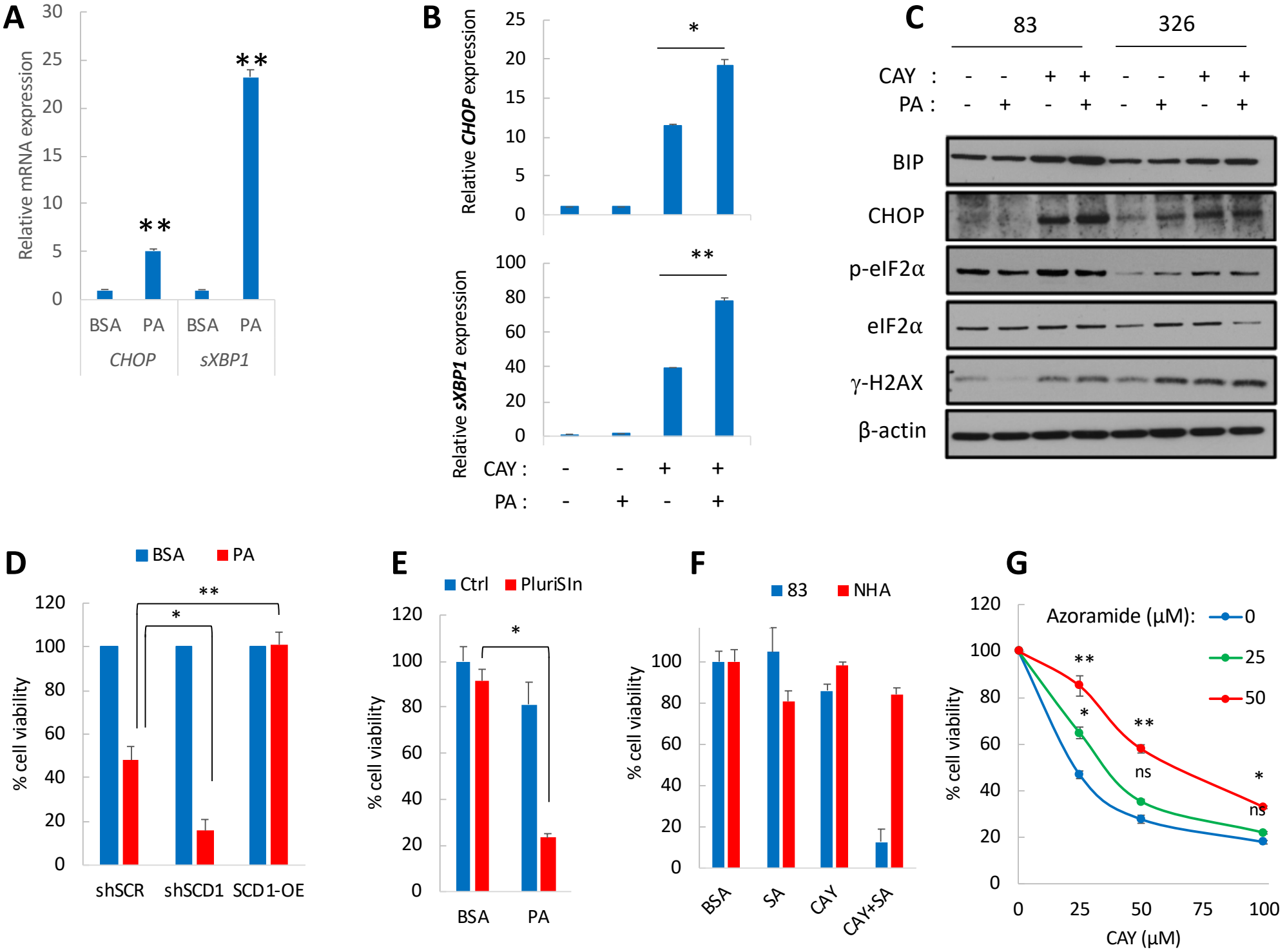
A
Relative mRNA expression
30
25
20
15
10
5
0
**
**
BSA
PA
BSA
PA
CHOP
sXBP1
B
Relative CHOP expression
25
20
15
10
5
0
*
Relative sXBP1 expression
100
80
60
40
20
0
**
CAY : - - + +
PA : - + - +
C
83
326
CAY : - - + + - - + +
PA : - + - + - + - +
BIP
CHOP
p-eIF2α
eIF2α
γ-H2AX
β-actin
D
BSA
PA
% cell viability
120
100
80
60
40
20
0
**
*
shSCR
shSCD1
SCD1-OE
E
Ctrl
PluriSIn
% cell viability
120
100
80
60
40
20
0
*
BSA
PA
F
83
NHA
% cell viability
100
80
60
40
20
0
BSA
SA
CAY
CAY+SA
G
Azoramide (μM): 0
25
50
% cell viability
120
100
80
60
40
20
0
**
*
**
ns
*
ns
0
25
50
75
100
CAY (μM)

Figure S4: SCD1 inhibition promotes ER stress. Related to Figure 4. **A.** Relative mRNA expression of the ER stress markers *CHOP* and *sXBP1* in 83 GSCs treated with PA (400 μM) for 24h. **B.** Relative mRNA expression of *CHOP* and *sXBP1* in 83 GSCs treated with CAY (50nM) and PA (50 μM) for 24h. **C.** Immunoblot analysis of the indicated ER stress and DNA damage markers in two GSCs treated with CAY (50nM) and PA (50 μM) for 24h. **D.** Cell viability in GSCs expressing shSCR, shSCD1 or SCD1-OE and treated with PA (200 μM) for 4 days. **E.** Cell viability in GSCs treated with PluriSIn (1 μM) in the presence or absence of PA (50 μM) for 3 days. **F.** 83 GSCs and NHA co-treated with CAY (10nM for 83 and 1 μM for NHA) and Stearic Acid (SA; 200 μM). Cell viability was measured after 4 days. **G.** Treatment of GSCs with Azoramide (25-50 μM) protects against CAY-induced cell death. *$p<0.05$; **$p<0.001$; ns: not significant; Student t-test.

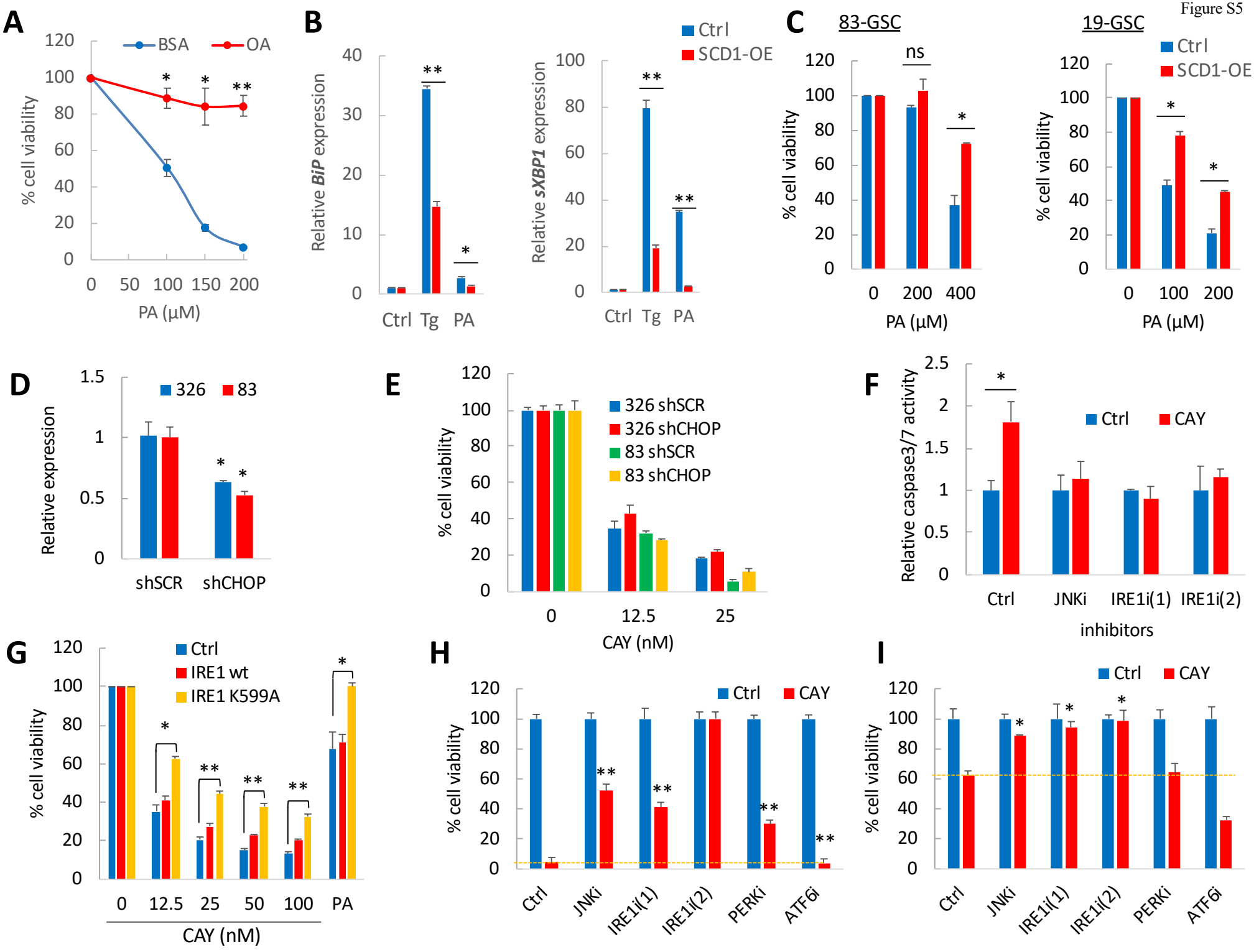
A
BSA
OA
% cell viability
PA (μM)
B
Relative BiP expression
Relative sXBP1 expression
Ctrl
SCD1-OE
Ctrl Tg PA
C
83-GSC
19-GSC
ns
% cell viability
PA (μM)
D
326
83
Relative expression
shSCR shCHOP
E
326 shSCR
326 shCHOP
83 shSCR
83 shCHOP
% cell viability
CAY (nM)
F
Relative caspase3/7 activity
Ctrl
CAY
Ctrl JNKi IRE1i(1) IRE1i(2)
inhibitors
G
Ctrl
IRE1 wt
IRE1 K599A
% cell viability
CAY (nM)
H
Ctrl
CAY
% cell viability
Ctrl JNKi IRE1i(1) IRE1i(2) PERKi ATF6i
I
Ctrl
CAY
% cell viability
Ctrl JNKi IRE1i(1) IRE1i(2) PERKi ATF6i

Figure S5: SCD1-mediated UFA synthesis mitigates ER stress and protects from UPR-induced apoptotic signaling. Related to Figure 4. **A.** Treatment of GSCs with OA (50 μM) protects against PA-induced cell death assessed 4 days after treatment. **B.** Relative mRNA expression of *sXBP1* and *BiP* in GSCs expressing an empty vector (Ctrl) or SCD1 and treated with Thapsigargin (Tg; 300nM) or PA (400 μM). **C.** SCD1 overexpression protects against PA-mediated cell death as shown in 2 GSCs specimens. **D.** mRNA expression of CHOP following shRNA mediated knockdown of this gene in 2 GSCs. **E.** Silencing of CHOP fails to alter CAY-mediated cytotoxicity in 2 GSCs as detected by measuring cell viability 4 days after treatment. **F.** Fold change in caspase 3/7 activation after treatment with CAY (50nM) in the presence of JNK inhibitor (SP 600125; 20 μM) or IRE1 inhibitors (4μ8C: 25 μM and KIRA6: 5 μM). **G.** 83 GSCs stably expressing a control vector, IRE1 (wild-type) or mutant IRE1 K599A were treated with CAY or PA (300 μM). Cell viability was assessed after 3 days. **H-I.** Cell viability of 83 (H) and L0 (I) GSCs treated with CAY (50nM) or the combination of CAY with: JNK inhibitor (SP 600125; 20 μM), IRE1 inhibitors (4μ8C: 25 μM and KIRA6: 5 μM), PERK inhibitor (GSK2656157; 10 μM) and ATF6 inhibitor (Ceapin A7: 20 μM) for 4 days. *$p<0.05$; **$p<0.001$; ns: not significant; Student t-test.

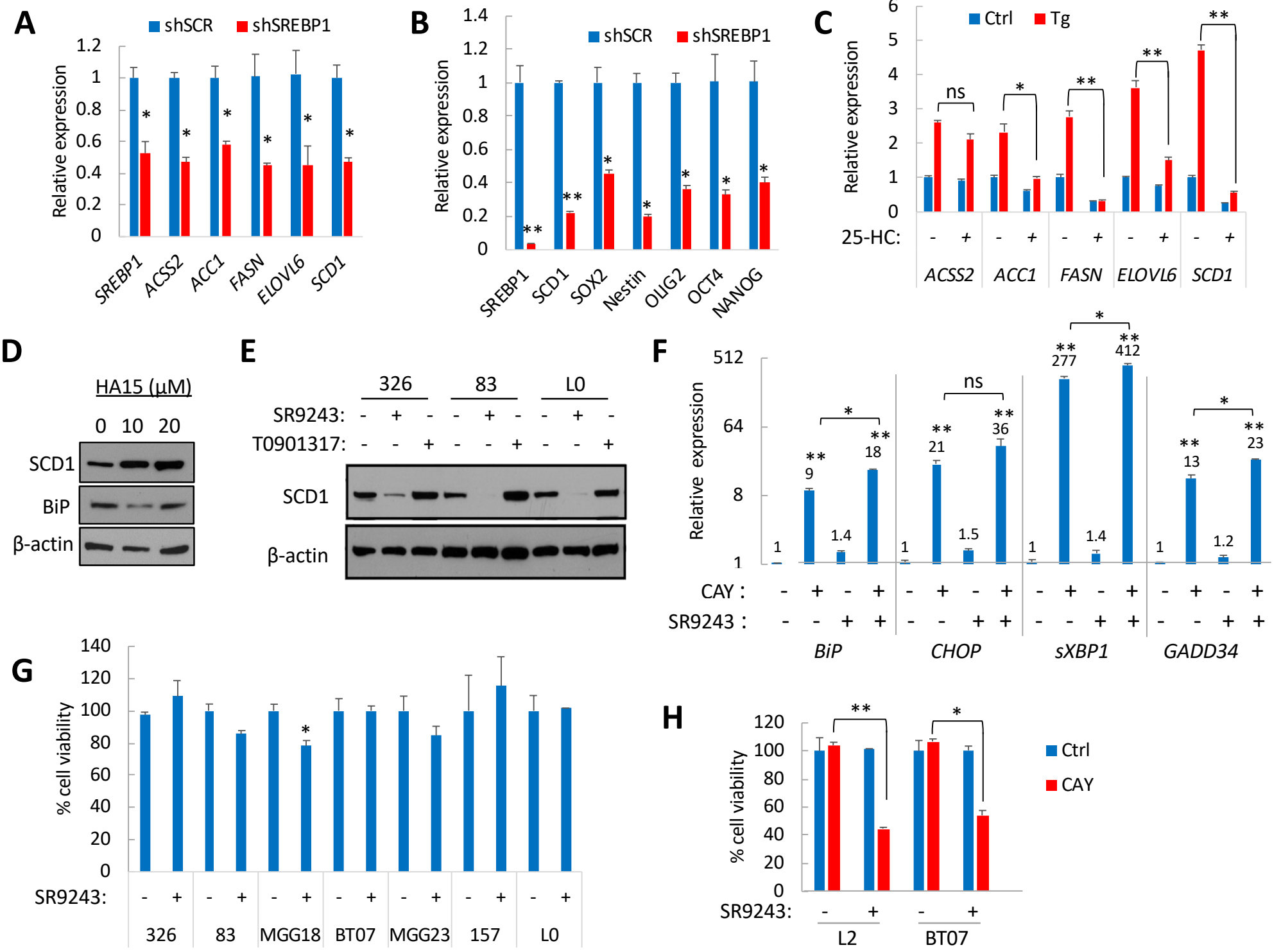
A
shSCR
shSREBP1
Relative expression
SREBP1
ACSS2
ACC1
FASN
ELOVL6
SCD1
B
shSCR
shSREBP1
Relative expression
SREBP1
SCD1
SOX2
Nestin
OLIG2
OCT4
NANOG
C
Ctrl
Tg
Relative expression
25-HC:
ACSS2
ACC1
FASN
ELOVL6
SCD1
D
HA15 (μM)
0 10 20
SCD1
BiP
β-actin
E
326
83
L0
SR9243:
T0901317:
SCD1
β-actin
F
Relative expression
CAY :
SR9243 :
BiP
CHOP
sXBP1
GADD34
G
% cell viability
SR9243:
326
83
MGG18
BT07
MGG23
157
L0
H
% cell viability
Ctrl
CAY
SR9243:
L2
BT07

Figure S6. ER stress promotes SCD1 expression through SREBP1 activation. Related to Figures 5. **A.** Relative expression of SREBP1 target genes after shRNA-mediated silencing of SREBP1 in 326-GSCs. **B.** Relative expression of SREBP1, SCD1 as well as the stem cell markers *SOX2*, *NESTIN*, *OLIG2*, *OCT4* and *NANOG* in BT07 GSCs expressing shSREBP1. **C.** Relative expression of SREBP1 target genes in GSCs treated with Tg (300nM) in the presence or absence of 25-HC (50 μM). **D.** Immunoblot analysis of SCD1 and BiP expression in GSCs treated with HA15 at the indicated doses. **E.** Immunoblot analysis of SCD1 expression in GSCs treated with SR9243 (20 μM) or T0901317 (25 μM) for 24h. **F.** mRNA expression of ER stress markers following treatment with CAY (100nM) and SR9243 (20 μM) for 48h. **G.** Cell viability of the indicated GSCs specimens after treatment with SR9243 (20 μM) for 5 days. **H.** Two GSCs were treated with CAY (25nM) and SR9243 (10 μM), and cell viability was assessed after 4 days. *$p<0.05$; **$p<0.001$; Student t-test.

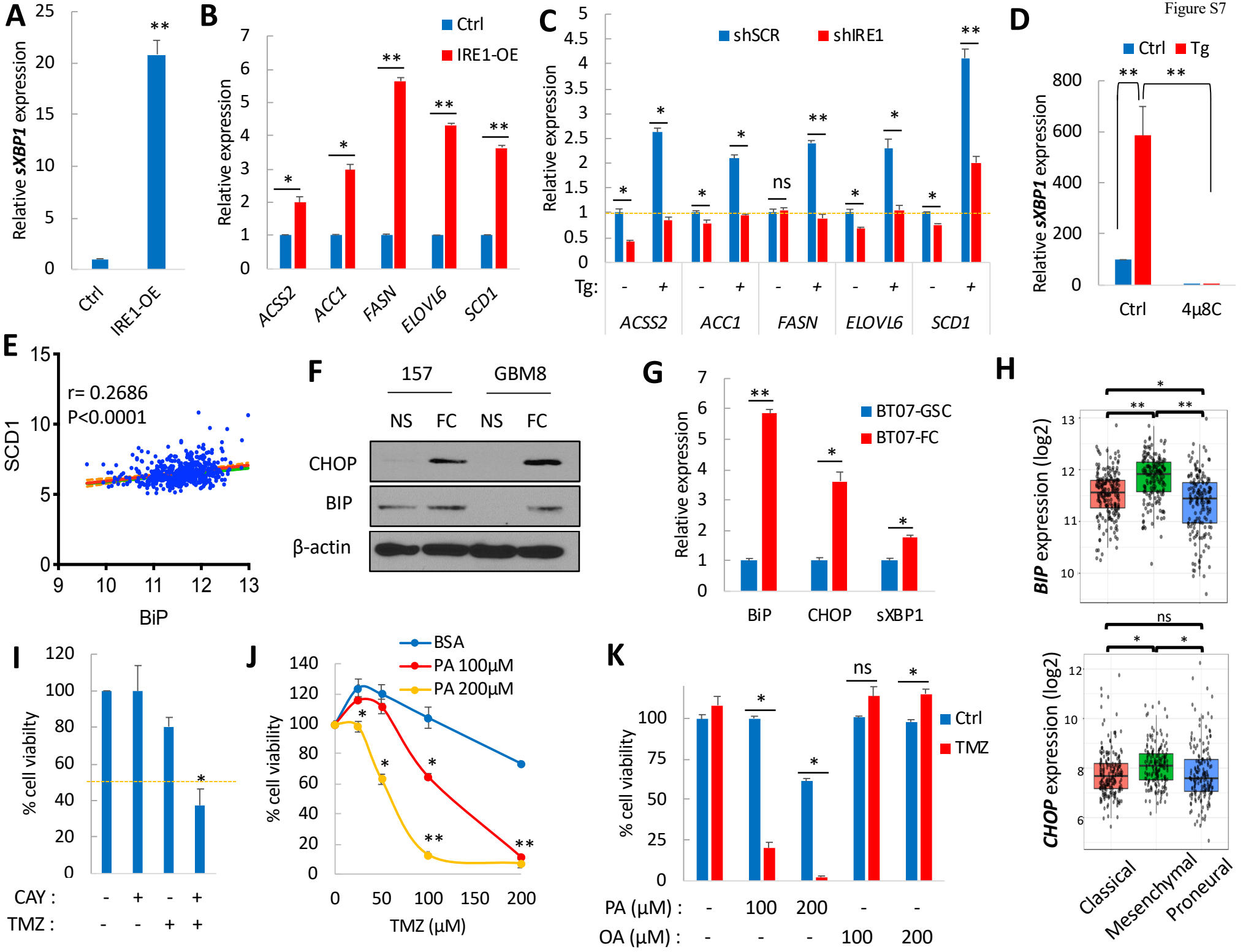
A
Relative sXBP1 expression
Ctrl
IRE1-OE
B
Relative expression
Ctrl
IRE1-OE
ACSS2
ACC1
FASN
ELOVL6
SCD1
C
Relative expression
shSCR
shIRE1
Tg:
ACSS2
ACC1
FASN
ELOVL6
SCD1
D
Relative sXBP1 expression
Ctrl
Tg
Ctrl
4μ8C
E
r= 0.2686
P<0.0001
SCD1
BiP
F
157
GBM8
NS
FC
NS
FC
CHOP
BIP
β-actin
G
Relative expression
BT07-GSC
BT07-FC
BiP
CHOP
sXBP1
H
BIP expression (log2)
CHOP expression (log2)
ns
Classical
Mesenchymal
Proneural
I
% cell viability
CAY :
TMZ :
J
BSA
PA 100μM
PA 200μM
% cell viability
TMZ (μM)
K
% cell viability
Ctrl
TMZ
PA (μM) :
OA (μM) :
ns

Figure S7: SCD1 is activated through ER stress-mediated IRE1 signaling and its inhibition sensitizes to TMZ. Related to Figures 6 and 7. **A.** Relative expression of *sXBP1* after doxycycline-induced expression of IRE1. **B.** Relative expression of SREBP1 target genes after IRE1 expression. **C.** Relative mRNA expression of SREBP1 target genes in GSCs transduced with shSCR or shIRE1 and subsequently treated with Tg (300nM). **D.** Relative expression of *sXBP1* after treatment with Tg (300nM) and the IRE1 inhibitor 4μ8C (25 μM) for 24h. **E.** SCD1 mRNA expression in the TCGA GBM dataset (n= 528 patients; platform: HG-133A) positively correlates with BiP expression. **F.** Immunoblot analysis for BiP and CHOP expression in two GSCs and their matching FC. **G.** mRNA expression of BIP, CHOP and sXBP1 in BT07 GSC and their FC. **H.** mRNA expression of *BiP* and *CHOP* in GBM subtypes from the TCGA dataset and plotted using Gliovis data portal. **I.** Cell viability in TMZ-resistant MGG23 GSCs pretreated with CAY (50 nM) for 24h followed by TMZ (200 μM) for 5 days. **J.** Treatment of L0 GSCs with PA increases the cytotoxicity of TMZ (200 μM). Cell viability was measured 5 days after treatment. **K.** Cell viability of L1 GSCs treated with TMZ (200 μM) in combination with PA or OA at the indicated doses for 4 days. *$p<0.05$; **$p<0.001$; ns: not significant; Student t-test.

SUPPLEMENTAL EXPERIMENTAL PROCEDURES

Cell culture

Primary GBM cells used in this study were derived from surgical specimens obtained from GBM patients at the Massachusetts General Hospital (provided by Dr. Hiroaki Wakimoto) under the appropriate Institutional Review Board approval or provided by Dr. Ichiro Nakano (GSCs: 157, 19, 326, 83, 1123) and Dr. Brent Reynolds (GSCs: L0, L1, L2). All specimens used in this study have been previously characterized (see table below) (Wakimoto et al., 2009; Wakimoto et al., 2012) (Mao et al., 2013) (Siebzehnrubl et al., 2013) (Teng et al., 2017). Cells were expanded as neurospheres and maintained in DMEM/F12 medium supplemented with B27 without vitamin A (1:50; Life Technologies), heparin (2 µg/mL; Sigma Aldrich), human recombinant EGF (20 ng/mL; ABM) and human recombinant bFGF-2 (10ng/mL; ABM). ReNcell VM (Millipore) were expanded under similar conditions. Primary human astrocytes were purchased from ScienCell and cultured in complete astrocyte medium (ScienceCell). All cells were maintained at 37°C in humidified 5% CO_2 incubators and regularly tested for potential mycoplasma contamination.

Specimen	diagnosis	SOX2	CD44	EGFR	Subtype	Reference
MGG18	GBM		+	ND	PN	Wakimoto et al.,2009, 2012
MGG8	GBM	+	-	ND	PN	Wakimoto et al.,2009, 2012
MGG23	GBM	-	+	ND	M	Wakimoto et al.,2009, 2012
BT07	GBM	+	-	ND	PN	Teng et al., 2017
83	GBM	-	+	+	M	Mao et al., 2013
326	N/A	-	+	+	M	Mao et al., 2013
1123	Gr III Oligo,1p19q del	-	+	+	M	Mao et al., 2013
157	GBM	+	-	-	PN	Mao et al., 2013
19	GBM	+	-	-	PN	Mao et al., 2013
L0	GBM	+	-	+	M-like	Siebzehnrubl et al., 2013
L1	GBM	+	+	+	M-like	Siebzehnrubl et al., 2013
L2	GBM	+	-	+	M-like	Siebzehnrubl et al., 2013

Patient derived GSCs were classified into Proneural (PN), Mesenchymal (M) or Mesenchymal-like based on the predominant expression of PN markers or M markers. The expression profile of SOX2, CD44 and EGFR is indicated as follows: High (+), low (-) or Intermediate (+/-). ND: Not determined.

Floating cells subpopulations

Floating cells (FC) collection and culture was performed as previously described (Teng et al., 2017). In brief, GSCs were cultured as monolayer in the presence of 10% fetal bovine serum (FBS) for 7-10 days. Non-adherent cells (FC) were collected from the supernatant and pelleted by centrifugation. Single FC were then expanded in serum-free stem cell medium.

Chemical reagents and Antibodies

CAY10566 was purchased from Cayman and Glixx Labs. Ceapin A7 (ATF6i) was provided by Dr. Peter Walter (Gallagher et al., 2016). The following compounds were obtained from Cayman Chemicals: PluriSIn; 4µ8C; KIRA6; GSK2656157; SP 600125; T0901317 and SR9243. MK-8245 and APO866 were obtained from SelleckChem, HA15, 25-Hydroxycholesterol and Thapsigargin from Sigma, Temozolomide from MedChemExpress. All fatty acids were obtained from Cayman and dissolved in DMSO to yield a stock concentration of 500mM- 3M. Fatty acids stocks were

subsequently complexed to fatty acid-free Bovine Serum Albumin (BSA; 2.5mM; Gold Biotechnology) and added to the culture medium.
The following antibodies were purchased from Cell Signaling Technologies: SCD1 (2438); BiP (3177); phospho SAPK/JNK (9255); SAPK/JNK (9252); phospho-eIF2α (3597); γ-H2AX (9718); Nestin (4760); β-actin (3700); Anti-rabbit IgG, HRP-linked Antibody (7074) and Anti-mouse IgG, HRP-linked Antibody. Rad51 (BSM-51402M) and IRE1 (BS-8680R) were obtained from BIOSS Antibodies, CHOP (sc-7351) from Santa Cruz, SOX2 (ab97959), Nestin (ab22035) and eIF2α (ab169528) from AbCam.

DNA constructs and Lentiviral vectors
To generate a lentiviral vector expression SCD1, the human SCD1 open reading frame was amplified by PCR (plasmid template obtained from the DNA Resource Core at Harvard Medical School, HMS) and subcloned into a CSCW-IRES-CFP lentivirus backbone thus generating CSCW-SCD1-IRES-CFP. This construct was verified by restriction digestion and sequencing.
CSCW-Fluc-IRES-mCherry lentivirus vector carrying an expression cassette for firefly luciferase (Fluc) and mCherry fluorescent protein was used for in vivo imaging. CSCW-IRES-CFP or pHAGE-CMV-MCS-IRES-ZsGreen (obtained from DNA Resource core, HMS) were used as control lentivirus vectors in all experiments. Doxycycline-inducible IRE1 wild-type (IRE1) or a kinase/endoribonuclease-inactive dominant-negative IRE1 (IRE1-K599A) were a gift from Fumihiko Urano (Addgene plasmids 20744 and 20745(Lipson et al., 2008)). Transcriptional activity was induced by treatment with Doxycycline (10 μM; Cayman) for at least 24h.
The following shRNA bacterial glycerol stocks: shSCD1 (TRCN0000327814), shSREBF1 (TRCN0000434619), shCHOP (TRCN0000364393), shIRE1 (TRCN0000000529) as well as a non-targeting control shRNA (pLKO.1-puro Non-Target shRNA Control) were obtained from Sigma (MISSION® shRNA Library), amplified and packaged into lentivirus vectors. GSCs were stably transduced with shRNA lentivirus and selected using puromycin (1 μg/mL). Knockdown efficiency was determined using immunoblotting and/or qRT-PCR.

Mass spectrometry profiling of Fatty acids
Fatty acids were analyzed as methyl ester derivatives (FAME) using gas chromatography/mass spectrometry (GC/MS) analysis. Sample preparation and fatty acid analysis were performed at the Small Molecule Mass Spectrometry Facility (Harvard University). GSCs were treated with CAY for 48 hours, cells were counted and fixed with methanol then dehydrated using a freeze-dry cycle. For extraction and preparation of fatty acids, samples were resuspended in methanol (500 μl) prior to adding the internal standard d27C14 (2mg/mL), hexane (400 μl) and acetyl chloride (100 μl). Samples were then vortexed, incubated in an ultrasound water bath with glass beads for 10 min followed by a 15 min incubation at 105°C. After an overnight incubation at 4 °C, hexane (500 μl) and water (1mL) were added and mixed. The hexane phase was separated by 10 min centrifugation (4000 rpm) and evaporated to dryness under N2 flow. Sample were resuspended in hexanes (100 μl) and ran on a Thermo Q exactive GC Orbitrap GC-MS/MS System. A FAME standard (Sigma) was run after all the samples to confirm ID of the FAME detected in the samples.
To determine an approximate comparison of concentrations of different fatty acids, we calculated an estimated normalized response as follows: 1. Since C14 is constant between samples, each area is divided by the area of C14 in the same sample. This should correct for biomass/extraction differences. This is a normalized area. 2. Using the standard reference, we calculated the ratio between normalized area and the known concentration of those fatty acids in the standard. 3. For fatty acids not present in the reference standard, the normalization factors are estimated by taking the factor corresponding to the fatty acid in the standard that is the closest (in number of carbon and insaturation). 4. Estimated normalized response is calculated for all the fatty acid. This is only an estimation, so small difference in response between fatty acids within a sample are not significant. 5. Difference between samples for each individual fatty acid are not dependent on this estimated response factor and are therefore significant.

ELDA assay
Stem cell frequency was calculated using the extreme limiting dilution analysis (ELDA) algorithm(Hu and Smyth, 2009) (http://bioinf.wehi.edu.au/software/elda/index.html). GSCs were dissociated then cells were counted and seeded into a 96-well plate at different cell numbers in 8-replicates. After 7-10 days, neurospheres of > 50 μm in diameter were counted. To determine secondary sphere formation, GSCs were dissociated into single cells and plated in eight replicates at a density of 1 cell per μl. Neurospheres were counted after 7-10 days.

Quantitative RT-PCR
Total RNA isolation was performed with RNeasy kit (Qiagen) followed by reverse transcription with OneScript cDNA synthesis Kit (ABM). qPCR reactions were performed using PowerUp SYBR Green Master Mix (Thermo Fisher) in a QuantStudio 3 Real-Time PCR system (AppliedBiosystems). All primer sequences used in this study are listed in

the table below. Oligonucleotides were synthesized by the CCIB DNA Core Facility at the Massachusetts General Hospital. qPCR runs included both human β-actin and HPRT as internal normalization controls.

GENE	Forward primer 5'	Reverse primer 5'	Source/Reference
SCD1	TCTAGCTCCTATACCACCACCA	TCGTCTCCAACTTATCTCCTCC	MGH primer bank
BiP (GRP78,	CATCACGCCGTCCTATGTCG	CGTCAAAGACCGTGTTCTCG	MGH primer bank
CHOP	GGAAACAGAGTGGTCATTCCC	CTGCTTGAGCCGTTCATTCTC	MGH primer bank
sXBP1	GGTCTGCTGAGTCCGCAGCAGG	GGGCTTGGTATATATGTGG	Hirota et al., 2006
GADD34	AGCCACGGAGGATAAAAGAACA	CTGAACGATACTCCCAGGACC	MGH primer bank
IRE1	CATCCCCATGCCGAAGTTCA	CTGCTTCTCTCCGGTCAGGA	MGH primer bank
SREBP1	ACAGTGACTTCCCTGGCCTAT	GCATGGACGGGTACATCTTCAA	MGH primer bank
NAMPT	CGGCAGAAGCCGAGTTCAA	GCTTGTGTTGGGTGGATATTGTT	MGH primer bank
FASN	AAGGACCTGTCTAGGTTTGATGC	TGGCTTCATAGGTGACTTCCA	MGH primer bank
ACC1	GCAGGTCACACGTCTCTTTAT	CCAGCCTGTCATCCTCAATATC	This paper
ACSS2	AAAGGAGCAACTACCAACATCTG	GCTGAACTGACACACTTGGAC	MGH primer bank
ELOVL6	AACGAGCAAAGTTTGAACTGAGG	TCGAAGAGCACCGAATATACTGA	MGH primer bank
SOX2	AACCCCAAGATGCACAACTC	GCTTAGCCTCGTCGATGAAC	MGH primer bank
NESTIN	AACAGCGACGGAGGTCTCTA	TTCTCTTGTCCCGCAGACTT	MGH primer bank
OCT4	AGTGAGAGGCAACCTGGAGA	ACACTCGGACCACATCCTTC	MGH primer bank
NANOG	TTCCTTCCTCCATGGATCTG	TCTGCTGGAGGCTGAGGTAT	MGH primer bank
OLIG2	CTCCTCAAATCGCATCCAGA	AGAAAAAGGTCATCGGGCTC	MGH primer bank
ACTB	CATGTACGTTGCTATCCAGGC	CTCCTTAATGTCACGCACGAT	MGH primer bank
HPRT	CCTGGCGTCGTGATTAGTGAT	AGACGTTCAGTCCTGTCCATAA	MGH primer bank

TCGA analysis

Datasets for mRNA expression and survival of GBM patients were obtained from the TCGA using Gliovis data portal (Bowman et al., 2017). Data plotting and statistical analysis were performed using GraphPad Prism.

SUPPLEMENTAL REFERENCES:

Bowman, R. L., Wang, Q., Carro, A., Verhaak, R. G., and Squatrito, M. (2017). GlioVis data portal for visualization and analysis of brain tumor expression datasets. Neuro-oncology *19*, 139-141.

Gallagher, C. M., Garri, C., Cain, E. L., Ang, K. K., Wilson, C. G., Chen, S., Hearn, B. R., Jaishankar, P., Aranda-Diaz, A., Arkin, M. R.*, et al.* (2016). Ceapins are a new class of unfolded protein response inhibitors, selectively targeting the ATF6alpha branch. Elife *5*.

Hu, Y., and Smyth, G. K. (2009). ELDA: extreme limiting dilution analysis for comparing depleted and enriched populations in stem cell and other assays. Journal of immunological methods *347*, 70-78.

Lipson, K. L., Ghosh, R., and Urano, F. (2008). The role of IRE1alpha in the degradation of insulin mRNA in pancreatic beta-cells. PloS one *3*, e1648.

Mao, P., Joshi, K., Li, J., Kim, S. H., Li, P., Santana-Santos, L., Luthra, S., Chandran, U. R., Benos, P. V., Smith, L.*, et al.* (2013). Mesenchymal glioma stem cells are maintained by activated glycolytic metabolism involving aldehyde dehydrogenase 1A3. Proceedings of the National Academy of Sciences of the United States of America *110*, 8644-8649.

Siebzehnrubl, F. A., Silver, D. J., Tugertimur, B., Deleyrolle, L. P., Siebzehnrubl, D., Sarkisian, M. R., Devers, K. G., Yachnis, A. T., Kupper, M. D., Neal, D.*, et al.* (2013). The ZEB1 pathway links glioblastoma initiation, invasion and chemoresistance. EMBO Mol Med *5*, 1196-1212.
Teng, J., Carla da Hora, C., Kantar, R. S., Nakano, I., Wakimoto, H., Batchelor, T. T., Chiocca, E. A., Badr, C. E., and Tannous, B. A. (2017). Dissecting inherent intratumor heterogeneity in patient-derived glioblastoma culture models. Neuro-oncology *19*, 820-832.
Wakimoto, H., Kesari, S., Farrell, C. J., Curry, W. T., Jr., Zaupa, C., Aghi, M., Kuroda, T., Stemmer-Rachamimov, A., Shah, K., Liu, T. C.*, et al.* (2009). Human glioblastoma-derived cancer stem cells: establishment of invasive glioma models and treatment with oncolytic herpes simplex virus vectors. Cancer research *69*, 3472-3481.
Wakimoto, H., Mohapatra, G., Kanai, R., Curry, W. T., Jr., Yip, S., Nitta, M., Patel, A. P., Barnard, Z. R., Stemmer-Rachamimov, A. O., Louis, D. N.*, et al.* (2012). Maintenance of primary tumor phenotype and genotype in glioblastoma stem cells. Neuro-oncology *14*, 132-144.